École Polytechnique Fédérale de Lausanne

Master project in Physics

Low-dimensional population dynamics of spiking neurons via eigenfunction expansion

Carried out at **LCN**

Under the supervision of **Dr. Tilo Schwalger**

Done by

Noé Gallice

Under the direction of

Prof. Wulfram Gerstner and **Prof. Matthieu Wyart**

External Expert **Dr. Maurizio Mattia**

June 22, 2018

Acknowledgments

During this thesis, I have received great help from a lot of people and I would like to express my gratitudes for their time.
In particular I would like to thank Prof. Wulfram Gerstner director of the Laboratory of Computational Neuroscience and Prof. Matthieu Wyart director of the Laboratory of Physics of Complex Systems for their support, their critical comments which helped me to organize my thought, and for stimulating my curiosity during their lectures.
I am incredibly grateful to Dr. Tilo Schwalger, who guided me through this thesis, had always time for me despite his busy schedule and even from the other side of the Atlantic was always there to offer his advice, and his ideas. Working by his side has been a great experience and I have learned immensely from him.
Then I thank all the members of the LCN lab. They created a very friendly atmosphere. This allowed me to do my master project in the best possible conditions. And I would like to adress a special thanks to Dr. Samuel Muscinelli and to Dr. Vasiliki Liakoni for their time and their very wise advices.
Finally I liked to thank my parents, my sister and my brother who have always supported me.

Abstract

A low-dimensional population dynamics of spiking neurons is derived via eigenfunction expansion of the refractory density. As a result, an infinite dimension integral formulation is simplified to a three dimensional dynamical system by considering only the two slowest modes of the expansion. The validity of the derived approximation is shown for a large homogeneous population of Poisson neurons with absolute refractoriness. However, the presented results apply to a wide class of neuronal networks.

Contents

Chapter 1

Introduction

This thesis is concerned with the mean activity of large homogeneous population of neurons. In the brain billions of neurons form complex networks, they communicate with each other by short electrical pulses called spike or action potential. Neurons encode stimuli by emitting spikes trains in response to sensory inputs. To uncover the corresponding neural code, the analysis of spike statistics is essential.

One of the most common ways to model large neuronal networks is to use a simplification called a firing rate model. It is equivalent to a mean field approach where rather than recording the spiking trains of every single neuron, one tracks the averaged behavior of the spike rates of groups of neurons.

But can we predict the population activity $A(t)$ from the properties of its individual neurons? And how does the population activity respond to a novel input? Those are the question we might ask, when we pass from a microscopic description to a macroscopic description as illustrated in Fig.1.1.

Firing rate models provide simple models which are computationally efficient and are mathematically tractable to study the response of a population to an external input. The resulting models involves a compromise between accuracy and simplicity. Simple firing-rate models where the dynamics was governed by only one time constant fail to replicate certain dynamic features of populations of spiking neurons. To explain some phenomenological properties, heuristic model where developed but these model were not derived from the spiking neuron dynamics. [Wilson and Cowan (1972),Ostojic and Brunel (2011)].

In this project we consider a large homogeneous population of neurons modeled by time dependent renewal process. A common approach to recover the activity of such a population is based on the refractory density [Gerstner (2000), Chizhov and Graham (2007), Chizhov and Graham (2008), Schwalger et al. (2017)]. But the integral formulation present in the refractory density equation makes this approach computationally inefficient and limit the analytical tractability. Therefore the goal of this work is to derive a low-dimensional population dynamics of spiking neurons, starting from a spectral expansion of the refractory density equation. Thus we will first introduce in Sections 1.1 and 1.3, renewal processes and the refractory density approach. Then we will recall some properties of the spectral expansion in Section 1.4, which in previous studies was used to approximate the dynamics

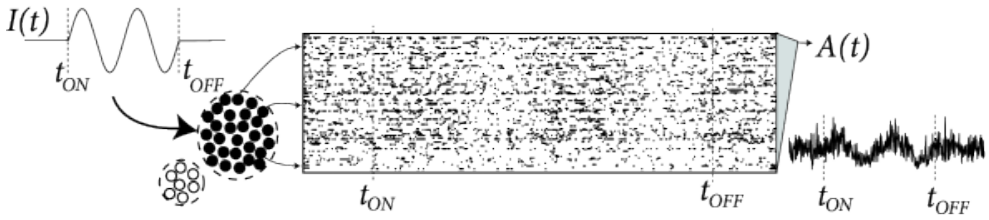

Figure 1.1: Response of population to a signal $I(t)$, represented by a sinusoidal modulation of the input starting at t_{ON} and ending at t_{OFF}, stimulates the population of 8000 excitatory neurons in a randomly coupled network of 8000 excitatory and 2000 inhibitory neurons (left). Each neuron produces a spike train (middle) illustrated here by lines of dots, each dot corresponding to a spike. Only 1% of the population is shown. At the macroscopic level, the population activity $A(t)$ (right) counts spikes in time bins of 1 ms averaged over the 8000 excitatory neurons. [Gerstner et al. (2014)]

of spiking networks, taking as state variable the membrane potential v [Mattia and Del Giudice (2002), Schaffer et al. (2013), Augustin et al. (2017)].

1.1 Renewal processes

A neuron model tells how an input is transformed into output spikes. We define $h(t)$ as the input potential, its time derivative is given by

$$\tau_m \dot{h} = -h + \mu(t) + RI_{syn}(t) \tag{1.1}$$

where $\mu(t)$ represents an external stimulus, and I_{syn} is the synaptic current, due to the spikes from other neurons.
Renewal processes keep memory of the last event,i.e. the last firing time $\hat{t}$. The age, i.e the time elapsed since the last spike $\tau = t - \hat{t}$, is a state variable of the neuron. For those processes the spikes are generated according to a stochastic intensity called the hazard rate $\rho(\tau, h)$. The hazard rate $\rho(\tau, h)$ define the probability to spike between $t + \Delta t$ knowing that there were no spike between t and $\hat{t}$
To generate a spike train according to the hazard rate $\rho(\tau, h)$ in a simulation, one would proceed as follows

- At each time step Δt knowing the age τ of the neuron and the current input potential $h(t)$ the probability of a neuron to spike would be given by

$$p_{spike} = 1 - \exp(-\rho(\tau, h)\Delta t) \tag{1.2}$$

  We see that the probability to spike is 0 for $\rho(\tau, h) = 0$ and goes to 1 for $\rho(\tau, h) \to +\infty$

- When the neuron spikes, the age is reset to 0, otherwise the age variable would be incremented by Δt.

1.1.1 Interval distribution and Survivor function

Let us in this section assume a time-homogeneous process, i.e. $h = const$. We can calculate the interspike interval (ISI) density $P(\tau, h)$ i.e the probability to spike at age τ.

$$\int_0^\infty P(\tau, h)\mathrm{d}\tau = 1 \tag{1.3}$$

The interval distribution $P(\tau, h)$ is a probability density, which implies that integration of $P(\tau, h)$ over age yields a probability. The probability that a neuron which has fired a spike at $\hat{t}$ and fires the next spike between $\hat{t}$ and t is given by $\int_0^\tau P(s, h)\mathrm{d}s$.
The interspike-interval (ISI) distribution can be linked to the survivor function

$$S(\tau, h) = 1 - \int_0^\tau P(s, h)\mathrm{d}s \tag{1.4}$$

The survivor function $S(\tau, h)$ defines the probability that a neuron reaches the age τ, so that a neuron "survive" without firing between $\hat{t}$ and t. $P(\tau, h)$ describes the probability to spike at age τ. There it can be expressed as the product of the probability to survive until age τ times the momentary hazard $\rho(\tau, h)$.

$$P(\tau, h) = \rho(\tau, h)S(\tau, h) \tag{1.5}$$

The derivation of Eq.(1.4) yields to

$$P(\tau, h) = -\frac{\mathrm{d}}{\mathrm{d}\tau}S(\tau, h) \tag{1.6}$$

Inserting Eq.(1.5) in Eq.(1.6), we find that the hazard rate $\rho(\tau, h)$ corresponds to the rate of decay of the survivor function

$$\rho(\tau, h) = -\frac{\frac{\mathrm{d}}{\mathrm{d}\tau}S(\tau, h)}{S(\tau, h)} \tag{1.7}$$

Integrating eq.1.7 yields to the survivor function

$$S(\tau, h) = \exp\big[-\int_0^\tau \rho(s, h)\mathrm{d}s\big] \tag{1.8}$$

Inserting Eq.(1.8) in Eq.(1.5) the interval distribution can be explicitly express in terms of the hazard, and is by itself normalized

$$P(\tau, h) = -\frac{\mathrm{d}}{\mathrm{d}\tau}S(\tau, h) = \rho(\tau, h)\exp\big[-\int_0^\tau \rho(s, h)\mathrm{d}s\big] \tag{1.9}$$

Each of the three function $\rho(\tau, h)$, $P(\tau, h)$ and $S(\tau, h)$ is sufficient to describe statistical properties of a renewal system.

1.1.2 Examples

Interval distribution and hazard functions have been measured in many experiments. Here are some examples that will be useful for finding analytical approximations and/or that agree with experimental measurements.

Simple model with recovery function

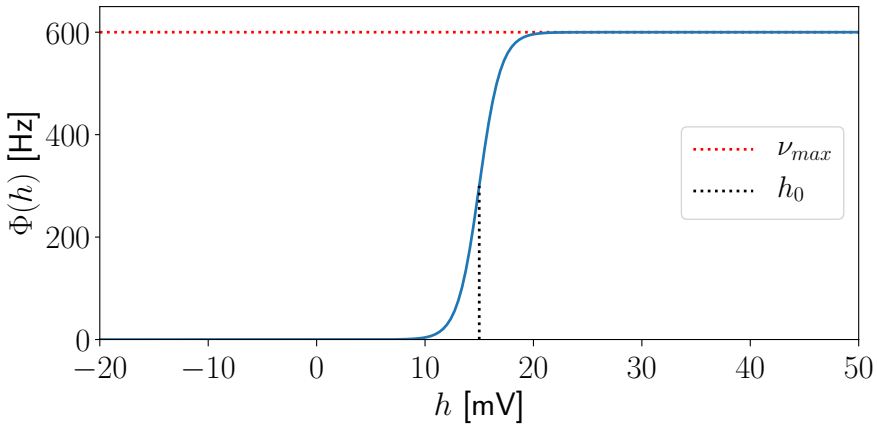

Figure 1.2: Rate $\Phi(h)$ as a function of input potential h. With $h_0 = 15$ mV , $\beta = 1$ mV^{1} and $\nu_{max} = 0.6$ kHz.

The hazard rate, can be expressed as a product of the instantaneous rate $\Phi(h)$ with a recovery function $g(\tau)$

$$\rho(\tau, h) = \Phi(h)g(\tau) \tag{1.10}$$

The function $\Phi(h)$ is a monotonically increasing function. In our examples we will use a sigmoidal function with threshold h_0 illustrated on Fig.1.2. For $h >> h_0$ the firing rate goes to the value ν_{max} for $h << h_0$ it goes to 0.

$$\Phi(h) = \frac{\nu_{max}}{1 + \exp[-\beta(h - h_0)]} \tag{1.11}$$

The hazard rate, the survival probability, and the interval distribution are shown in Fig.1.3 for two examples of recovery function g, with potential $h = h_0$ i.e $\Phi(h) = \frac{\nu_{max}}{2}$. Fig.1.3(a) corresponds to a Poisson process with absolute refractory period Δ:

$$g(\tau) = \theta(\tau - \Delta) \tag{1.12}$$

$\theta(\tau - \Delta)$ denotes the Heaviside function. The recovery function for Fig.1.3(b) is given by

$$g(\tau) = [1 - \exp(-\eta(\tau - \Delta))]\,\theta(\tau - \Delta) \tag{1.13}$$

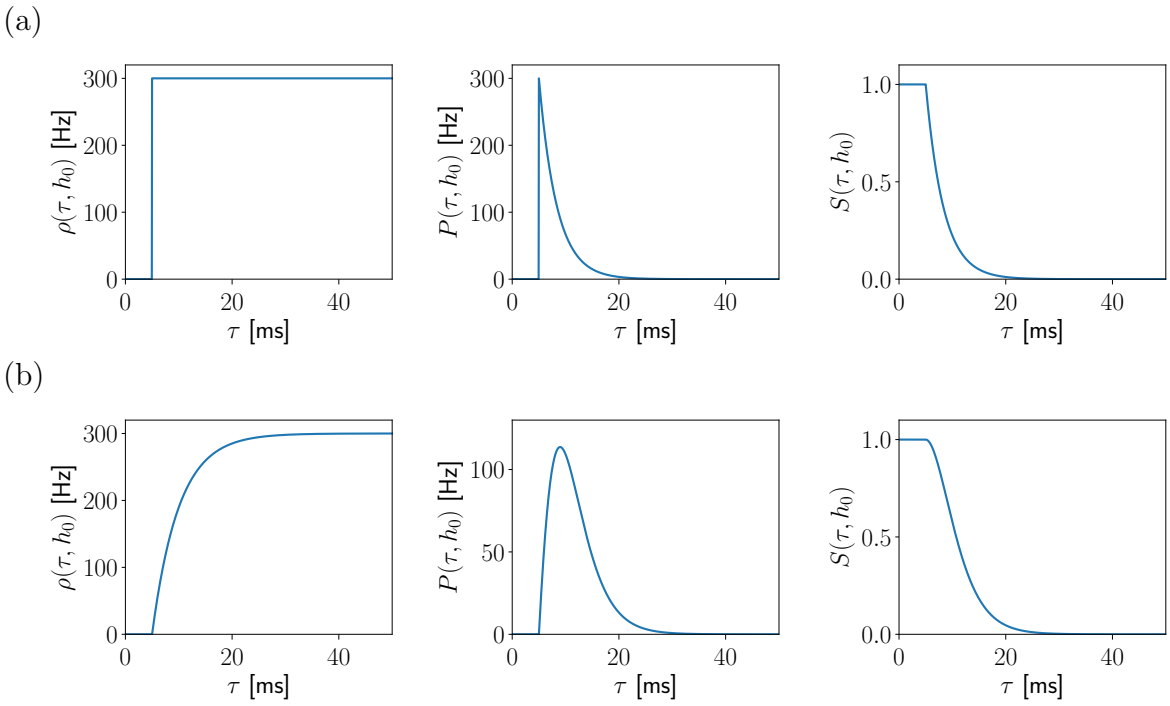

Figure 1.3: Hazard rate $\rho(\tau, h)$ (left), interval distribution $P(\tau, h)$ (middle) and survivor function $S(\tau, h)$ (right) for different recovery function $g(\tau)$. (a) Recovery function for a Poisson neuron with absolute refractoriness Δ, with $\Delta = 5$ ms, $h = h_0$, $\nu_{max} = 600$ Hz. (b) Recovery function defined by Eq.(1.13) with $\Delta = 5$ ms, $h = h_0$, $\nu_{max} = 600$ Hz.

The main difference is that for the Poisson neuron with absolute refractoriness the recovery function Eq.(1.12) make a jump, whereas in Eq.(1.13) the transition is smooth which gives rise to relative refractoriness. The time course of the recovery function given by Eq.(1.13), approximate well the recovery function measured for auditory neurons of the guinea-pig [Prijs et al. (1993)]

Gamma neuron model

The gamma neuron model is often used to model spike trains as it is one of the easiest non-Poisson process to analyze. For this neuron model the interspike distribution is given by

$$P(\tau) = \frac{\beta^\gamma}{\Gamma(\gamma)} \tau^{\gamma-1} e^{-\beta\tau} \tag{1.14}$$

Where $\beta := \beta(h)$ is a rate which depend on the input potential h
The rate of this neuron model is $R = \beta/\gamma$, And the coefficient of variation is given by $C_V = \gamma^{-\frac{1}{2}}$. For $\gamma = 1$ this corresponds to a Poisson process. For $C_V > 1$ the interspike distribution diverges as τ goes to 0. One can see the gamma neuron model as a succession of γ states where each state is a Poisson neuron with firing rate β since one has to pass by

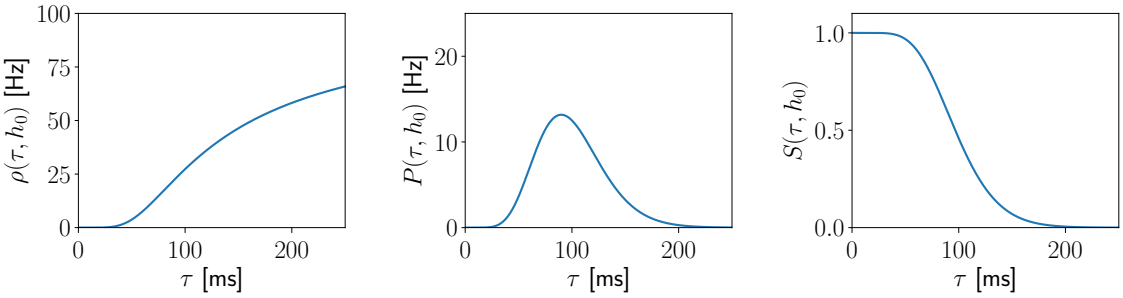

Figure 1.4: **Gamma neuron model.** Hazard rate $\rho(\tau, h)$ (left), interval distribution $P(\tau, h)$ (middle) and survivor function $S(\tau, h)$ (right) for a Gamma neuron model with $\beta = 100$ Hz and $\gamma = 10$

each state before spiking, this implies that the global rate of the total chain is $R = \beta/\gamma$, and induces relative refractoriness as shown on Fig.1.4.

Perfect integrate-and-fire model driven by white noise

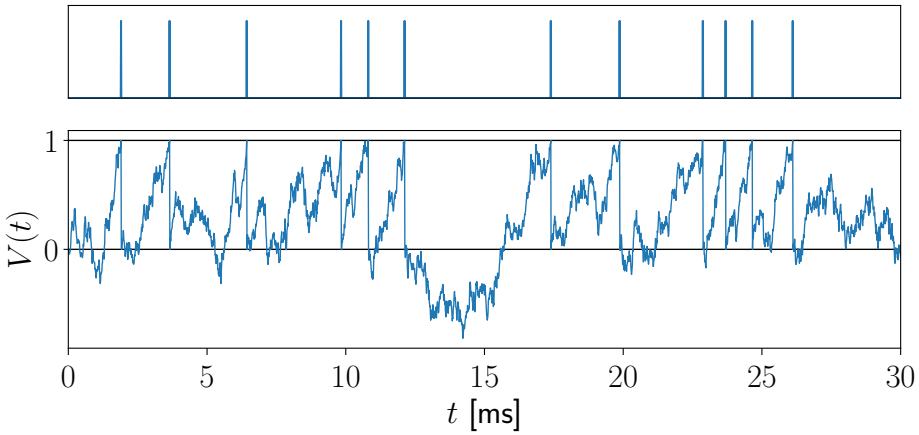

Figure 1.5: Typical realization $V(t)$ for the PIF model driven with a white noise with $f(h) = 0.3$ V_{th}, $D = 0.1$ V_{th}^2,$\tau_v = 1$ ms $V_{th} = 1$. The generated spike train is indicated on the top.

The perfect integrating-and fire model has been used to explain statistics of isolated neurons. The membrane potential V of a neuron can be seen as a Brownian-motion with drift $f(h)$ driven by a white noise, which is reset to the value V_r when it hits the threshold V_{th}. The function $f(h)$ is a mean current which depends on the input potential h.

$$\tau_v \dot{V} = f(h) + \sqrt{2D}\xi(t), \qquad if \quad V = V_{th} \quad V \to V_r \tag{1.15}$$

$$\langle \xi(t)\xi(s) \rangle = \delta(t - s) \tag{1.16}$$

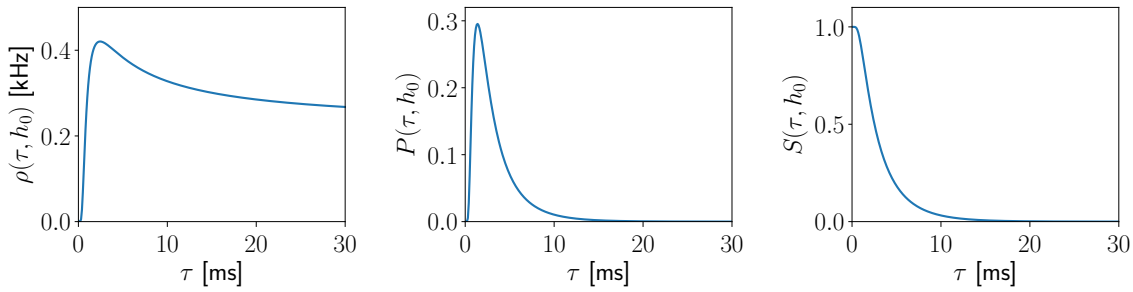

Figure 1.6: **PIF neurons.** Hazard rate $\rho(\tau, h)$ (left), interval distribution $P(\tau, h)$ (middle) and survivor function $S(\tau, h)$ (right) for the PIF model driven with a white noise with $f(h) = 0.3\ V_{th}$, $D = 0.1\ V_{th}^2$,$\tau_v = 1$ ms $V_{th} = 1$

A typical realization of the dynamics of $V(t)$ for a single neuron and the corresponding spike train is illustrated on Fig.1.5. The statistics of such neurons are shown on Fig.1.6. For this neuron model the interspike distribution is given by

$$P(\tau, h) = \frac{V_{th}\tau_v}{\sqrt{4\pi D\tau^3}} \exp\left(-\frac{(f(h)\tau - V_{th}\tau_v)^2}{4D\tau}\right) \tag{1.17}$$

The rate of this neuron model is $R = \frac{f(h)}{V_{th}\tau_v}$, And the coefficient of variation is given by $C_V = \sqrt{\frac{2D}{\tau_v f(h) V_{th}}}$.

1.2 Moment of the interspike interval distribution $P(\tau)$

For the upcoming theoretical derivations, it is usefull to introduce the moment of the interspike interval distribution. For a stationary spike train, the ISI distribution is also stationary. Here h is constant, so we used the notation $P(\tau)$ instead of $P(\tau, h)$. The interval distribution allows to compute the $k-$th moment,

$$\langle \tau^k \rangle = \int_0^\infty \tau^k P(\tau) \mathrm{d}\tau \tag{1.18}$$

It is useful to introduce the Laplace transform

$$P_L(\lambda) = \int_0^\infty \mathrm{d}\tau e^{-\lambda\tau} P(\tau) \tag{1.19}$$

from which the $k-$th ISI moment can be generated

$$\langle \tau^k \rangle = (-1)^k \frac{\mathrm{d}^k P_L}{\mathrm{d}\lambda^k}\Big|_{\lambda=0} \tag{1.20}$$

Hence, $P_L(\lambda)$ is called the ISI moment generating function. We can generated from this function the ISI cumulants defined by

$$\kappa_k = (-1)^k \frac{\mathrm{d}^k \ln P_L}{\mathrm{d}\lambda^k}\Big|_{\lambda=0} \tag{1.21}$$

The first two ISI cumulants are related to the ISI moments by

$$\kappa_1 = \langle \tau \rangle \tag{1.22}$$
$$\kappa_2 = \langle \tau^2 \rangle - \langle \tau \rangle^2 \tag{1.23}$$

The cumulants can be used to characterize the shape of the ISI density. The rate of a process R is given by

$$R = \langle \tau \rangle^{-1} = \kappa_1^{-1} \tag{1.24}$$

An important measure that quantify the variability of ISI distribution is the coefficient of variation C_V defined as

$$C_V = \sqrt{\frac{\langle \tau^2 \rangle}{\langle \tau \rangle^2} - 1} = \frac{\sqrt{\kappa_2}}{\kappa_1} \tag{1.25}$$

A Poisson process produces distributions with $C_V = 1$ which indicate a highly irregular spike train. A value of $C_V > 1$, implies that a given spike train is less regular than a Poisson process with the same firing rate. If $C_V < 1$, then the spike train is more regular. Whereas $C_V = 0$ indicates a perfectly regular spike train.

1.3 Populations of neurons and refractory density equations

1.3.1 Population model

There are about a hundred billion neurons in the human brain, distributed in different brain area and which form elaborate neural networks. Within a brain area one can identify subregions and layers where neurons are organized in populations of cells with similar properties. Eloquent examples are barrel columns in the primary somatosensory cortex [Lefort et al. (2009)], and pools of motor neurons [Kandel et al. (2000)].
Given the large number of neurons in a population, rather than tracking the spiking of individual neurons, it is appealing to describe the mean activity. Fig.1.1 illustrate the transition from a microscopic to a macroscopic description. The theory of population dynamics dates back to the 1970s [Knight (1972), Wilson and Cowan (1972)] and modern variants are used to predict the temporal evolution of the activity $A(t)$ [Schwalger et al. (2017)]. In a network of N neurons the population activity $A(t)$ is defined as the proportion of active neuron. Denoting by t_j^f the firing time f of the neuron j, the activity can be expressed as

$$A(t) = \frac{1}{N} \sum_{j=1}^{N} \sum_{f} \delta(t - t_j^f) \tag{1.26}$$

where δ a dirac function.
We consider large homogeneous population of neurons i.e all neuron are identical and receive the same input potential, composed of an external input$\mu(t)$ and a synaptic input current I_{syn}, due to the spikes from other neurons.

$$RI_{syn}(t) = JA(t) \tag{1.27}$$

where J denotes the coupling constant with the units of voltage seconds. For the sake of simplicity we will consider all-to-all coupling, i.e. each neuron is coupled to each neuron and therefore receives the same input proportional to the mean activity.

1.3.2 Refractory density equation

An approach on the refractory density $q(\tau, t)$ let analyze the dynamic in an homogeneous population [Gerstner and Kistler (2002)]. $q(\tau, t)$ characterize the number of neuron at time t that are in a similar state of activity, i.e with age $\tau = t - \hat{t}$, where $\hat{t}$ is the last spike time of the neuron. The population activity is thus given by

$$A(t) = q(0, t) \tag{1.28}$$

As long as a neuron does not fire, the age τ increase at the speed of $\frac{\mathrm{d}\tau}{\mathrm{d}t} = 1$, therefore the flux along the refractory variable τ is simply $q(\tau, t)$ and the continuity equation is given by

$$\frac{\partial q}{\partial t} = -\frac{\partial q}{\partial \tau} \tag{1.29}$$

When a neuron fires, the trajectory along the refractory variable τ stops at the current value and "reappears" at $\tau = 0$. The instantaneous probability to fire is given by the hazard function $\rho(\tau, h)$.Therefore the loss per unit time is given by $-\rho(\tau, h)q()\tau, t)$ and the full dynamic is then given by the master equation:

$$\partial_t q(\tau, t) = -\partial_\tau q(\tau, t) - \rho(\tau, h)q(\tau, t) \tag{1.30}$$

The dynamics is schematized on Fig.1.7. At time t_j The proportion of neurons at age τ_i which are firing and will reappear at age 0, is given by $q(\tau_i, \tau_j)\rho(\tau_i, h_j)\Delta t$ (red arrow). The neuron that did not fire will reach the age τ_{i+1} at time t_{j+1} (blue arrow). The sum of all trajectories that "disappear" at time t due to firing, are "reappearing" at $\tau = 0$ since each neuron will fire at some finite time, the boundary conditions are

$$q(0, t) = \int_0^\infty \rho(\tau, h)q(\tau, t)d\tau = A(t) \tag{1.31}$$

$$q(\infty, t) = 0 \tag{1.32}$$

Additionally, q is normalized

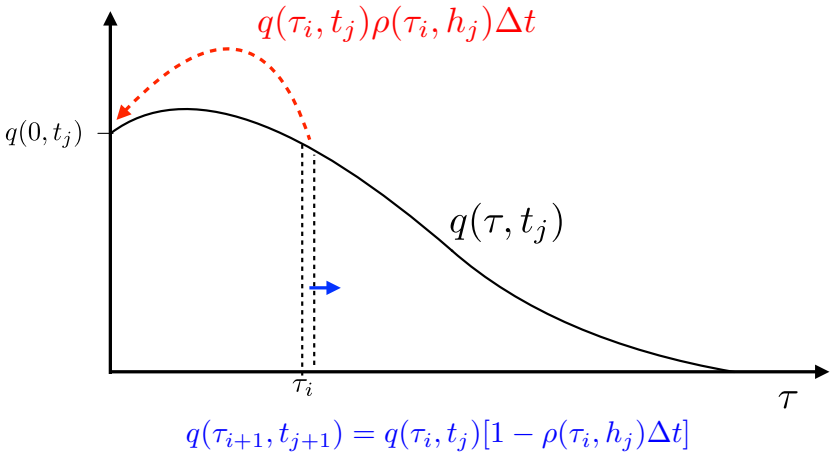

Figure 1.7: Scheme of refractory density dynamics. The red arrow represents the proportion of neurons with age τ_i whose fire at time t_j, the blue one represents those that are not firing and will reach the age τ_{j+1} at time t_{j+1}. Taking the limit $\Delta t \to 0$ yields to Eq.(1.30)

$$\int_0^\infty q(\tau, t)\mathrm{d}\tau = 1 \tag{1.33}$$

and has the initial density

$$q(\tau, 0) = q_0(\tau) \tag{1.34}$$

where $q_0(\tau)$ is some function that satisfies the conditions Eq.(1.31) and Eq.(1.33).

1.4 Spectral decomposition method

We apply a probability density approach, which describes the evolution of the density of states $q(x, t)$, in the phase space of a specific choice of neuronal state variable x. Many approaches consider only one state, the membrane potential v, governed by the integrate and fire model. In the refractory density approach, the state variable is the age τ, i.e the time elapsed since the last spike. Assuming that the state variable x can be described by a Markovian dynamics, we can write down an evolution equation for the state density q in the following form

$$\partial_t q(x, t) = \mathcal{L} q(x, t) \tag{1.35}$$

Where $\mathcal{L}$ is the evolution operator. Taking the membrane potential v as a state variable the evolution operator corresponds to the Fokker-Planck operator [Mattia and Del Giudice (2002),Schaffer et al. (2013)]. We will first recall some property for a general evolution operator.

1.4.1 General properties of the evolution operator

The operator $\mathcal{L}$ of Eq.1.35 has a set of eigenfunctions and associated eigenvalues

$$\mathcal{L}\left|\phi_n\right\rangle = \lambda_n \left|\phi_n\right\rangle \tag{1.36}$$

Where $|\phi_n\rangle = \phi_n(x,t)$ and $\lambda_n = \lambda_n(t)$. The time dependency provides a moving basis $\{|\phi_n\rangle\}$.
Because $\mathcal{L}$ is a real operator, if an eigenvalue λ_n is complex, its complex conjugate $\bar{\lambda}_n$ is also an eigenvalue of $\mathcal{L}$, with eigenfunction $|\bar{\phi_n}\rangle$. We will use the notation $\bar{\lambda}_n = \lambda_{-n}$, i.e the sums over the spectrum of $\mathcal{L}$ range over all integer numbers. Note that $\lambda_0 = 0$ is always an eigenvalue of the operator $\mathcal{L}$ and corresponds to the stationary solution.
Because $\mathcal{L}$ is not generally Hermitian we also need to define the eigenfunctions $|\psi_n\rangle$ of the adjoint operator $\mathcal{L}^+$

$$\mathcal{L}^+\left|\psi_n\right\rangle = \tilde{\lambda}_n \left|\psi_n\right\rangle \tag{1.37}$$

The adjoint operator is defined as $\langle\psi|\mathcal{L}\phi\rangle = \langle\mathcal{L}^+\psi|\phi\rangle$, where we introduce the inner product

$$\langle\psi|\phi\rangle = \int \psi(x,t)\phi(x,t)\mathrm{d}x \tag{1.38}$$

Using the properties of the operator, one can show that the eigenvalues of Eq.(1.36) and Eq.(1.37) are the same

$$\begin{aligned}
\lambda_n\langle\psi_n|\phi_n\rangle &= \int \psi_n(x,t)\mathcal{L}\phi_n(x,t)\mathrm{d}x \\
&= \langle\psi_n|\mathcal{L}\phi_n\rangle \\
&= \langle\mathcal{L}^+\psi_n|\phi_n\rangle \\
&= \int \mathcal{L}^+\psi_n(x,t)\phi_n(x,t)\mathrm{d}x \\
&= \tilde{\lambda}_n\langle\psi_n,|\phi_n\rangle
\end{aligned} \tag{1.39}$$

Eq.(1.39) implies that $\lambda_n = \tilde{\lambda}_n$ and

$$\mathcal{L}^+\left|\psi_n\right\rangle = \lambda_n \left|\psi_n\right\rangle \tag{1.40}$$

For different eigenvalues, the eigenfunctions ψ_i and ϕ_j are orthogonal

$$\begin{aligned}
\lambda_j\langle\psi_i|\phi_j\rangle &= \langle\psi_i|\mathcal{L}\phi_j\rangle \\
&= \langle\mathcal{L}^+\psi_i|\phi_j\rangle \\
&= \lambda_i\langle\psi_i|\phi_j\rangle
\end{aligned} \tag{1.41}$$

And with an appropriate normalization the two set of eigenfunctions are biorthonormal

$$\langle \psi_i | \phi_j \rangle = \delta_{ij} \tag{1.42}$$

The density of state $q(x,t)$ can be expressed in terms of this basis

$$|q\rangle = \sum_n a_n |\phi_n\rangle \tag{1.43}$$

where $a_n(t) = \langle \psi_n | q \rangle$ are the time dependent coefficients of the modal expansion. Since q is real, $\bar{a}_n = a_{-n}$.

1.4.2 Rate equation

The activity $A(t)$ can often be written as the action of some flux operator $\hat{J}$ on the density of states $q(x,t)$

$$A(t) = \hat{J} q(x,t) \tag{1.44}$$

Taking the membrane potential v as state variable, the flux operator $\hat{J}$ is defined as

$$\hat{J} q(v,t) = -D(v,t) \partial_v q(v,t)|_{v=v_{th}} \tag{1.45}$$

where D is a diffusion term caused by the shot-noise from presynaptic neurons and $\hat{J}q(v,t)$ denotes the fractions of realizations per unit time crossing the threshold v_{th}.
In the refractory approach with state variable τ, i.e the times elapsed since the last spike, Eq.(1.31) implies that $\hat{J}$ is given by

$$\hat{J} q(\tau,t) = \int_0^\infty \rho(\tau,t) q(\tau,t) \mathrm{d}\tau \tag{1.46}$$

Expanding the refractory density on the eigenfunction basis Eq.(1.43), Eq.(1.44) can be rewritten as

$$\begin{aligned} A(t) &= \sum_n a_n \hat{J} |\phi_n\rangle \\ &= \vec{a} \cdot \vec{f} \end{aligned} \tag{1.47}$$

where $\vec{a} = \{a_n\}$ and $\vec{f} = \{\hat{J}|\phi_n\rangle\}$ corresponds to the operator $\hat{J}$ acting on the eigenfunctions $\{|\phi_n\rangle\}$. The dynamics of the a_n can be determined directly from the evolution equation Eq.(1.35)

$$\begin{aligned} \dot{a}_n &= \langle \psi_n | \partial_t q \rangle + \langle \partial_t \psi_n | q \rangle \\ &= \langle \psi_n | \mathcal{L} q \rangle + \dot{h} \sum_m a_m \langle \partial_h \psi_n | \phi_m \rangle \\ &= \lambda_n a_n + \dot{h} \sum_m a_m \langle \partial_h \psi_n | \phi_m \rangle \end{aligned} \tag{1.48}$$

Here we have use the fact that the time dependence of ψ is due to the change of h, which is an external variable. The result is an emission rate equation

$$\dot{\vec{a}} = (\mathbf{\Lambda} + \boldsymbol{C}\dot{h})\vec{a} \tag{1.49}$$

$$A = \vec{a} \cdot \vec{f} \tag{1.50}$$

The synaptic coupling are expressed in the matrix $\boldsymbol{C}$: $C_{nm} = \langle \partial_h \psi_n | \phi_m \rangle$. And $\mathbf{\Lambda}$ is the diagonal matrix of the eigenvalues of $\mathcal{L}$: $\Lambda_{nm} = \lambda_n \delta_{nm}$

In previous studies a prominent choice of the state variable was the membrane potential v to analyze the dynamics of networks of integrate and fire neurons. In this case the evolution operator $\mathcal{L}$ was the Fokker-Planck operator [Mattia and Del Giudice (2002), Gerstner and Kistler (2002), Schaffer et al. (2013)]. However neurons with different refractory state can have the same potential, and thus the membrane potential can be a weak predictor of the neurons complete state, whereas the age approximates quite well the refractory states. This encourage the use of a refractory approach. In this study, we re-evalute the spectral decomposition for the refractory density Eq.(1.30).

1.5 Aim of the study

We consider a large homogeneous populations of neurons modeled by a time dependent renewal process. A common approach to recover the population activity is based on the refractory density using the age of a neuron at state variable, Section.1.3.2. There are nevertheless some limitations to this integral formulation of the activity Eq.(1.31). It has infinite dimension, it is not computationally efficient and the analytical tractability is limited.
Therefore the goal of this thesis is to derive a low-dimensional population dynamics keeping the first mode of the spectral expansion of the refractory density equation. In other words we would like to apply the eigenfunction expansion method presented in Section 1.4 to the operator of the refractory density. Therefore we will first introduce in Sections 2.1 and 2.2, the operator and adjoint operator of the refractory density and the corresponding eigenfunctions, to finally in Section 2.3 derive from this expansion a firing rate equation for a large homogeneous population of neurons.
In Chapter 3, we will present the spectrum for a specific model and an approximation of the first eigenvalue for a general renewal process. We will then show the accuracy of the derived approximation using as model a large homogeneous population of Poisson neurons with absolute refractoriness. In Chapter 4 we will first consider the uncoupled case and analyze the effect of the refractory period Δ. In Chapter 5 we will finally look at a network of synaptically coupled neurons.

Chapter 2

Theory

In this chapter we will follow the different steps of the spectral expansion presented in Section 1.4, defining the operator and adjoint operator of the refractory density equation. Thanks to the derived spectrum and biorthonormal basis, we will obtained a low dimensional firing rate equation.

2.1 Operator of the refractory density, and eigenvalue spectrum $\{\lambda_n\}$

The master equation Eq.(1.30) can be rewritten introducing the operator

$$\mathcal{L} = -\partial_\tau - \rho(\tau, h) \tag{2.1}$$

$$\partial_t q(\tau, t) = \mathcal{L} q(\tau, t) \tag{2.2}$$

The set of eigenfunctions and associated eigenvalues of $\mathcal{L}$ obeys

$$\mathcal{L} \left|\phi_n\right\rangle = \lambda_n \left|\phi_n\right\rangle \tag{2.3}$$

and respect the boundary conditions Eq.(1.31)

$$\phi_n(0, h) = \int_0^\infty \rho(\tau, h)\phi_n(\tau, h)\mathrm{d}\tau \tag{2.4}$$

$$\phi_n(\infty, h) = 0 \tag{2.5}$$

To lighten the notation, we will omit the dependence on h (the time dependent potential) of the hazard rate $\rho(\tau)$, the ISI distribution $P(\tau)$, the survivor function $S(\tau)$, and of the set of eigenfunctions $\{|\phi_n\rangle\}$ and eigenvalues $\{\lambda_n\}$.

The solution of Eq.(2.3) is

$$\begin{aligned}\phi_n(\tau) &= \phi_n(0)\exp\left(-\lambda_n\tau - \int_0^\tau \rho(s)\mathrm{d}s\right) \\ &= \phi_n(0)e^{-\lambda_n\tau}S(\tau)\end{aligned} \tag{2.6}$$

Inserting Eq.(2.6) in the boundary condition Eq.(2.4), we find the condition

$$\phi_n(0) = \int_0^\infty \mathrm{d}\tau\rho(\tau)\phi_n(0)\exp\left(-\lambda_n\tau - \int_0^\tau \rho(s)\mathrm{d}s\right) \tag{2.7}$$

which can be written as

$$1 = \int_0^\infty e^{-\lambda_n\tau}P(\tau)\mathrm{d}\tau = P_L(\lambda_n) \tag{2.8}$$

The condition Eq.(2.8) already derived in [Schwalger (2016)], states that the Laplace transform of the ISI density $P_L(\lambda)$ at the (complex) arguments λ_n must be unity.
We can conclude some properties of the spectrum λ_n imposed by Eq.(2.8) [Schwalger (2016)]

- As expected, the eigenvalue $\lambda_0 = 0$ fulfilled the condition because the ISI density is normalized. This eigenvalue corresponds to the stationary density.

- The real part of λ_n cannot be positive, as expected for physical reason. Indeed the solution of the refractory density equation is directly related to the eigenvalues of $\mathcal{L}$ and is expected to converge to ϕ_0, instead of exploding which would be the case for positive eigenvalues. In fact for $\Re(\lambda_n) > 0$,

  $$\int_0^\infty e^{-\lambda_n\tau}P(\tau)\mathrm{d}\tau < \int_0^\infty |e^{-\lambda_n\tau}|P(\tau)\mathrm{d}\tau < \int_0^\infty P(\tau)\mathrm{d}\tau = 1 \tag{2.9}$$

  which contradicts Eq.(2.8).

2.2 Adjoint operator $\mathcal{L}^+$, and normalization

Because $\mathcal{L}$ is not Hermitian we also need to define the set of eigenfunctions $\{|\psi_n\rangle\}$ of the adjoint operator $\mathcal{L}^+$

$$\mathcal{L}^+ |\psi_n\rangle = \lambda_n |\psi_n\rangle \tag{2.10}$$

We can find the adjoint operator $\mathcal{L}$, using integration by part

$$\begin{aligned}\langle\psi|\mathcal{L}\phi\rangle &= \int_0^\infty \psi(\tau)\mathcal{L}\phi(\tau)\mathrm{d}\tau \\ &= \int_0^\infty \psi(\tau)[-\partial_\tau - \rho(\tau)]\phi(\tau)\mathrm{d}\tau \\ &= -[\psi(\tau)\phi(\tau)]_0^\infty + \int_0^\infty \partial_\tau\psi(\tau)\phi(\tau)\mathrm{d}\tau - \int_0^\infty \rho(\tau)\psi(\tau)\phi(\tau)\mathrm{d}\tau \\ &= \psi(0)\phi(0) + \int_0^\infty [\partial_\tau - \rho(\tau)]\psi(\tau)\phi(\tau)\mathrm{d}\tau\end{aligned} \tag{2.11}$$

Using Eq.(1.31) to rewrite $\phi(0)$ as an integral yields

$$\begin{aligned}\langle\psi|\mathcal{L}\phi\rangle &= \int_0^\infty \psi(0)\rho(\tau)\phi(\tau)\mathrm{d}\tau + \int_0^\infty [\partial_\tau - \rho(\tau)]\psi(\tau)\phi(\tau)\mathrm{d}\tau \\ &= \int_0^\infty \big\{[\partial_\tau - \rho(\tau)]\psi(\tau) + \psi(0)\rho(\tau)\big\}\phi(\tau)d\tau \\ &= \langle\mathcal{L}^+\psi|\phi\rangle\end{aligned} \tag{2.12}$$

As we will later normalize the eigenfunction to obtain a biorthonormal basis we can for now set $\psi_n(0) = 1$, and the adjoint operator can be expressed as

$$\mathcal{L}^+\psi_n(\tau) = [\partial_\tau - \rho(\tau)]\psi_n(\tau) + \rho(\tau) \tag{2.13}$$

The un-normalized solution of Eq.(2.10) is thus

$$\begin{aligned}\psi_n(\tau) &= \exp\left(\lambda_n\tau + \int_0^\tau \rho(s)\mathrm{d}s\right)\left[1 - \int_0^\tau \mathrm{d}x\rho(x)\exp\left(-\lambda_n x - \int_0^x \rho(s)\mathrm{d}s\right)\right] \\ &= e^{\lambda_n\tau}\big[1 - \int_0^\tau \mathrm{d}xP(x)e^{-\lambda_n x}\big]\frac{1}{S(\tau)}\end{aligned} \tag{2.14}$$

In particular for $n = 0$, $\lambda_0 = 0$ and using Eq.(1.4) we have

$$\begin{aligned}\psi_0(\tau) &= \frac{1}{S(\tau)}\big[1 - \int_0^\tau P(x)\mathrm{d}x\big] \\ &= 1\end{aligned} \tag{2.15}$$

Inserting Eq.(2.6) and Eq.(2.14) in Eq.(1.42) yields the normalization of the biorthonormal basis

$$1 = \int_0^\infty \mathrm{d}\tau\phi_n(0)\left[1 - \int_0^\tau \mathrm{d}xP(x)e^{-\lambda_n x}\right] \tag{2.16}$$

$$\phi_n(0) = \frac{1}{\int_0^\infty \big[1 - \int_0^\tau P(x)e^{-\lambda_n x}\mathrm{d}x\big]\mathrm{d}\tau} \tag{2.17}$$

In particular for $n = 0$, $\lambda_0 = 0$ and using Eq.(1.4) we recover the relation

$$\phi_0(0) = \frac{1}{\int_0^\infty S(\tau)\mathrm{d}\tau} \tag{2.18}$$

which shows that the stationary rate $\phi_0(0)$ is the inverse of the mean time $\langle\tau\rangle$ to spike, given by $\langle\tau\rangle = \int_0^\infty S(\tau)\mathrm{d}\tau$.

2.3 Firing rate equation

The spectrum $\{\lambda_n\}$ of the operator $\mathcal{L}$ provides a moving basis $\{|\phi_n\rangle\}$. The refractory density $q(\tau, t)$ can be expressed with the eigenfunctions $\{|\phi_n\rangle\}$.

$$|q\rangle = \sum_n a_n |\phi_n\rangle \tag{2.19}$$

where $a_n(t) = \langle\psi_n|q\rangle$ are the time dependent coefficients of the modal expansion. In particular from Eq.(2.15), and Eq.(1.42) we have $a_0(t) = 1$. The dynamics of the a_n for $n \neq 0$ can be determined directly using Eq.(2.1), and Eq.(2.2) as derived in Eq.(1.48) Defining the coupling coefficient as

$$C_{nm} = \langle\partial_h\psi_n|\phi_m\rangle \tag{2.20}$$

we can rewrite Eq.(1.48)

$$\dot{a}_n = \lambda_n a_n + \dot{h}\sum_m C_{nm}a_m \tag{2.21}$$

Using Eq.(2.19), we can finally express the activity $A(t) = q(0, t)$ as

$$A(t) = \sum_n a_n(t)\phi_n(0) \tag{2.22}$$

We can explicitly separate the real part $X(t)$ and the imaginary part $Y(t)$ of $a_1(t)$, as well as the real part $\Phi_r(h)$ and the imaginary part $\Phi_i(h)$ of $\phi_1(0, h)$.

$$a_1(t) = X(t) + iY(t) \tag{2.23}$$
$$\phi_1(0, h) = \Phi_r(h) + i\Phi_i(h) \tag{2.24}$$

Keeping only the first mode, and using the fact that $|\phi_{-n}\rangle = |\bar{\phi}_n\rangle$ and $a_{-n} = \bar{a}_n$, Eq.(2.22) becomes

$$\begin{aligned} A(t) &= \phi_0(0) + a_1\phi_1(0) + a_{-1}\phi_{-1}(0) \\ &= \phi_0(0) + (X + iY)(\Phi_r + i\Phi_i) + (X - iY)(\Phi_r - i\Phi_i) \\ &= \phi_0(0) + 2(X\Phi_r - Y\Phi_i) \end{aligned} \tag{2.25}$$

And the dynamics of the a_1 is given by

$$\dot{a}_1 = \lambda_1 a_1 + \dot{h}\big[C_{10} + C_{11}a_1 + C_{1-1}a_{-1}\big] \tag{2.26}$$

Inserting Eq.(2.23) in Eq.(2.26) yields

$$\dot{X} + i\dot{Y} = \lambda_1(X + iY) + \dot{h}\big[C_{10} + C_{11}(X + iY) + C_{1-1}(X - iY)\big] \tag{2.27}$$

Separating the imaginary part and the real part of Eq.(2.27), we derive two first-order differential equations for the real part X and the imaginary part Y of a_1

$$\dot{X} = \Big(\alpha_r + (\beta_r + \gamma_r)\dot{h}\Big)\, X - \Big(\alpha_i + (\beta_i - \gamma_i)\dot{h}\Big)\, Y + \eta_r \dot{h} \tag{2.28}$$

$$\dot{Y} = \Big(\alpha_r + (\beta_r - \gamma_r)\dot{h}\Big)\, Y + \Big(\alpha_i + (\beta_i + \gamma_i)\dot{h}\Big)\, X + \eta_i \dot{h} \tag{2.29}$$

with

$$\alpha_r(h) = \Re[\lambda_1(h)] \tag{2.30}$$
$$\alpha_i(h) = \Im[\lambda_1(h)] \tag{2.31}$$
$$\beta_i(h) = \Re[C_{11}(h)] \tag{2.32}$$
$$\beta_r(h) = \Im[C_{11}(h)] \tag{2.33}$$
$$\gamma_r(h) = \Re[C_{1-1}(h)] \tag{2.34}$$
$$\gamma_i(h) = \Im[C_{1-1}(h)] \tag{2.35}$$
$$\eta_r(h) = \Re[C_{10}(h)] \tag{2.36}$$
$$\eta_i(h) = \Im[C_{10}(h)] \tag{2.37}$$

We have finally a set of three non linear differential equation $\dot{h}$, $\dot{X}$, $\dot{Y}$. The dynamics of the input potential h is given by Eq.(1.1). We can rewrite Eq.(2.25) making the dependence in time t and h explicit

$$A(t) = \phi_0(0, h(t)) + 2\big(X(t)\Phi_r(h(t)) - Y(t)\Phi_i(h(t))\big) \tag{2.38}$$

Chapter 3

Spectrum

In this chapter we will derive in Section 3.1, the eigenvalue spectrum $\{\lambda_n\}$ for different processes. In Section 3.2, we will present a derivation to obtain an approximation of the first eigenvalue λ_1 for a general process.

3.1 Spectral derivation for specific models

3.1.1 Poisson neuron with absolute refractoriness

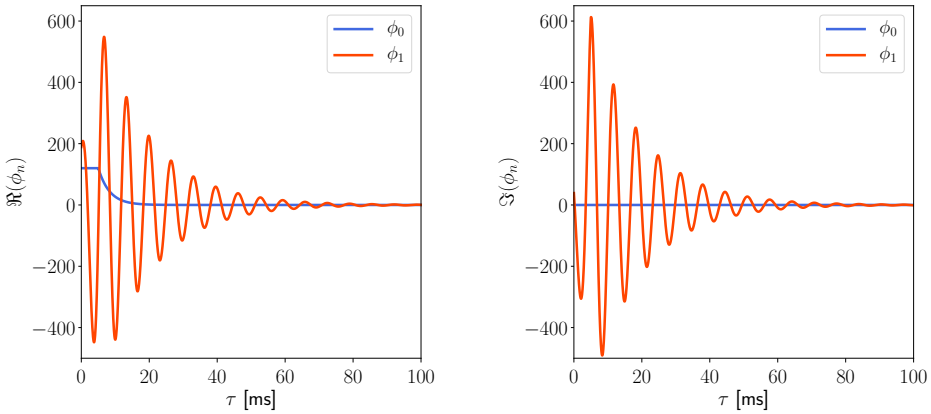

Figure 3.1: Real part (left) and imaginary part (right) of the eigenfunctions ϕ_n of the first modes $n = 0, 1$ for a **Poisson neuron with absolute refractory period** Δ. With $\Delta = 5$ ms, $h = h_0$, $\nu_{max} = 0.6$ kHz. ϕ_{-1} is the complex conjugate of ϕ_1

In this section we consider a Poisson neuron with absolute refractory period Δ, the hazard rate is defined by the recovery function Eq.(1.12). For the sake of simplicity in the notation we will use the variable ν such that $\nu = \Phi(h)$. The hazard rate is then given by

$$\rho(\tau, h) = \nu\,\Theta(\tau - \Delta) \tag{3.1}$$

And the interspike interval distribution is

$$P(\tau, h) = \nu \exp\big(-\nu(\tau - \Delta)\big)\Theta(\tau - \Delta) \tag{3.2}$$

For this process we can compute the Laplace transform of the ISI density

$$\begin{aligned} P_L(\lambda) =& \int_0^\infty P(\tau) e^{-\lambda\tau} \mathrm{d}\tau \\ =& \frac{\nu}{\nu + \lambda} \exp(-\lambda\Delta) \end{aligned} \tag{3.3}$$

By the change of variable $w_n = (\nu + \lambda_n)\Delta$, the normalization condition Eq.(2.8) $P_L(\lambda)) = 1$, can be rewritten as

$$\Delta\nu e^{\nu\Delta} = w_n e^{w_n} \tag{3.4}$$

The solution of equation Eq.(3.4) is given introducing the Lambert W-function $W(z, n)$

$$w_n = W(\Delta\nu e^{\nu\Delta}, n) \tag{3.5}$$

from which we read the eigenvalue spectrum $\{\lambda_n\}$

$$\lambda_n = \frac{1}{\Delta} W(\Delta\nu e^{\nu\Delta}, n) - \nu \tag{3.6}$$

We can explicitly express the eigenfunctions, $|\phi_n\rangle$ of the operator $\mathcal{L}$ and $|\psi_n\rangle$ of the adjoint operator $\mathcal{L}^+$

$$\phi_n(\tau) = \frac{\nu + \lambda_n}{1 + \Delta(\nu + \lambda_n)} e^{-\lambda_n\tau} \left[\Theta(\Delta - \tau) + \Theta(\tau - \Delta) e^{-\nu(\tau - \Delta)}\right] \tag{3.7}$$

These eigenfunctions are illustrated in Fig.3.1 for $n = 0, 1$

$$\begin{aligned} \psi_n(\tau) =& \Theta(\Delta - \tau) e^{\lambda_n\tau} + \Theta(\tau - \Delta) \frac{\nu}{\nu + \lambda_n} \\ =& \Theta(\Delta - \tau) e^{\lambda_n\tau} + \Theta(\tau - \Delta) e^{\lambda_n\Delta} \end{aligned} \tag{3.8}$$

One can verify that the set ofeigenfunctions satisfy Eq.(1.42). So far we considered constant h. For the general case of time-dependent input, we need we need to compute $\frac{d\psi_n(\tau)}{d\nu}$, to define the coupling coefficients Eq.(2.20).

$$\frac{\partial\psi_n(\tau)}{\partial\nu} = \frac{\lambda_n}{\nu[1 + \Delta(\nu + \lambda_n)]} \left[\Theta(\Delta - \tau)\tau e^{\lambda_n\tau} + \Theta(\tau - \Delta)\Delta e^{\lambda_n\Delta}\right] \tag{3.9}$$

The coupling coefficients are then given by

$$\begin{aligned} C_{nn} =& \frac{\partial \nu}{\partial h} \int_0^\infty \frac{d\psi_n(\tau)}{d\nu} \phi_n(\tau) d\tau \\ =& \frac{\lambda_n \Delta (1 + \frac{1}{2}\Delta(\nu + \lambda_n))}{\nu (1 + \Delta(\nu + \lambda_n))^2} \frac{\partial \nu}{\partial h} \end{aligned} \tag{3.10}$$

$$\begin{aligned} C_{nm} =& \frac{\partial \nu}{\partial h} \int_0^\infty \frac{d\psi_n(\tau)}{d\nu} \phi_m(\tau) d\tau \\ =& \frac{\lambda_n (\nu + \lambda_m)}{\nu (\lambda_n - \lambda_m)(\nu + \lambda_n)(1 + \Delta(\nu + \lambda_m))} \frac{\partial \nu}{\partial h} \end{aligned} \tag{3.11}$$

3.1.2 Gamma neuron model

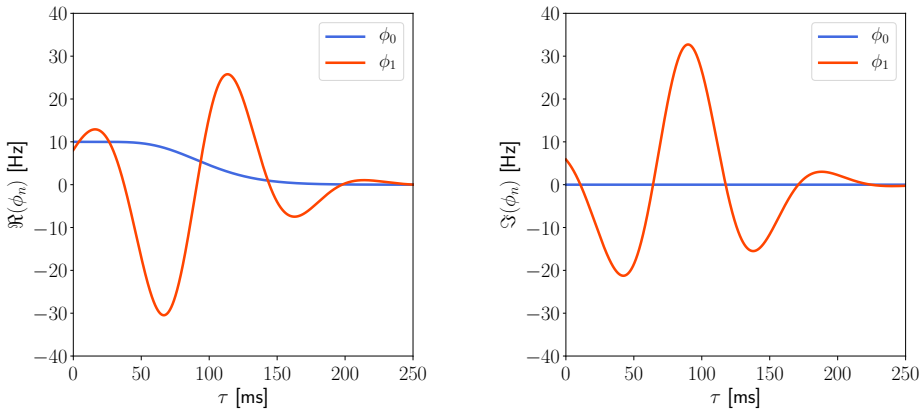

Figure 3.2: Real part (left) and imaginary part (right) of the eigenfunction ϕ_n of the first modes for a **Gamma neuron model** with $\beta = 100$ $\gamma = 10$. ϕ_{-1} is the complex conjugate of ϕ_1

In this section we consider a gamma neuron model. Taking the Laplace transform of the ISI density Eq.(1.14) yields

$$P_L(\lambda) = \left(\frac{\beta}{\beta + \lambda} \right)^\gamma \tag{3.12}$$

The condition given by Eq.(2.8) leads then to the solutions [Schwalger (2016)]

$$\lambda_n = \beta \left(\exp\left(\frac{2\pi i}{\gamma} n \right) - 1 \right), \qquad n = 0, ..., \gamma - 1 \tag{3.13}$$

Interestingly the gamma neuron model has a finite number of mode. Eq.(3.13) can be rewritten in function of the rate R and the coefficient of variation C_V as

$$\lambda_n = RC_V^{-2}\left(\exp\left(2\pi i C_V^2 n\right) - 1\right) \tag{3.14}$$

And the normalization Eq.(2.15) yields to

$$\phi_n(0) = \frac{1}{\gamma\beta^\gamma(\beta+\lambda_n)^{-(\gamma+1)}} \tag{3.15}$$

The eigenfunctions of the gamma neuron model are illustrated in Fig.3.2 for $n = 0, 1$.

3.1.3 PIF model

In this section we will consider the perfect integrating and fire neuron modem. The Laplace transform of the ISI density Eq.(1.17) is

$$P_L(\lambda) = \exp\big(\frac{f(h)V_{th}\tau_v}{2D}\big[1 - \sqrt{1 + \frac{4D\lambda}{f(h)^2}}\big]\big) \tag{3.16}$$

The condition given by Eq.(2.8) leads then to the solutions

$$\lambda_n = -\frac{4\pi D}{\tau_V^2 V_{th}^2}n^2 + \frac{f(h)}{V_{th}\tau_v}ni \tag{3.17}$$

The spectrum can be rewritten as a function of the rate R and the coefficient of variation C_V

$$\lambda_n = -2\pi^2 RC_V^2 n^2 + 2\pi R i\, n \tag{3.18}$$

We could not find an analytical solution for the normalization equation Eq.(2.16).

3.2 A general approximation of the spectrum

In the previous sections we derived the spectrum $\{\lambda_n\}$ for different specific neuron models. But for a general ISI distribution $P(\tau)$, it is not always possible to obtained a analytical form of the Laplace transform $P_L(\lambda)$. Thats why we would like to find a method to approximate the first eigenvalue λ_1. From Eq.(1.20) one can see that the the Laplace transform of the ISI distribution can be rewritten with the cumulant κ_n as

$$P_L(\lambda) = \exp\left[\sum_{k=1}^{+\infty}(-1)^k\kappa_k\frac{\lambda^k}{k!}\right] \tag{3.19}$$

The condition $P_L(\lambda_n) = 1 = \exp(2\pi\imath n)$ Eq.(2.8) can be rewritten as

$$\sum_{k=1}^{+\infty}(-1)^k\kappa_n\frac{\lambda_n^k}{k!}=2\pi in \tag{3.20}$$

We can approximate the first eigenvalue λ_1, neglecting the terms multiplied by the cumulants κ_k for $k>2$. Consequently Eq.(3.20) becomes

$$\frac{\kappa_2}{2}\lambda_1^2-\kappa_1\lambda_1-2\pi i=0 \tag{3.21}$$

λ_1 correspond to the roots of Eq.(3.21) with the negative real parts, as we have shown before in Section 2.1, a positive real part would be unphysical and does not satisfy Eq.(2.8). The approximation of λ_1 can be rewritten in terms of the rate R and the coefficient of variation C_V using Eq.(1.24) and Eq.(1.25)

$$\lambda_1\simeq RC_V^{-2}\left(1-\sqrt{1+4\pi iC_V^2}\right) \tag{3.22}$$

In Schaffer et al. (2013), they determined the first eigenvalue λ_1 for different renewal processes by fitting the dependency of the real part and the imaginary part on the rate R and on the coefficient of variation squared C_V^2. They found as a relationship for small C_V:

$$\lambda_1\simeq -R\left(\left(\frac{C_V}{0.22}\right)^2+2\pi i\right) \tag{3.23}$$

Note that for small C_V we can Taylor expand the square root in Eq.(3.22) and recover an expression close to Eq.(3.23)

$$\lambda_1\simeq -R\left(2\pi^2C_V^2+2\pi i\right)+\mathcal{O}(C_V^4) \tag{3.24}$$

Indeed $\frac{1}{(0.22)^2}\simeq 20.7$ and $2\pi^2\simeq 19.7$.

Fig.3.3 shows the relative error $\frac{|\lambda_1-\hat{\lambda}_1|}{|\lambda_1|}$ for the different approximation $\hat{\lambda}_1$ of the first eigenvalue λ_1.

For the Gamma neuron model the relative error is below 0.1 for $C_V<0.3$ for the approximation obtained by Schaffer et al Eq.(3.23) and the one given by Eq.(3.22). For $C_V<0.1$ Eq.(3.22) is a better approximation.

For the PIF neuron model, the κ_2 approximation has a relative error below 0.1 for $C_V<0.1$. It becomes better than the Schaffer approximation for $C_V<0.1$. Actually Eq.(3.24) is exact thus for small C_V, the relative error with the κ_2 is very low and we saw that the Schaffer approximation is close to this expression, so even for large C_V the Schaffer approximation is good.

It seems that the truncation of the cumulant sum to second order gives a good approximation of the first eigenvalue λ_1 for small C_V.

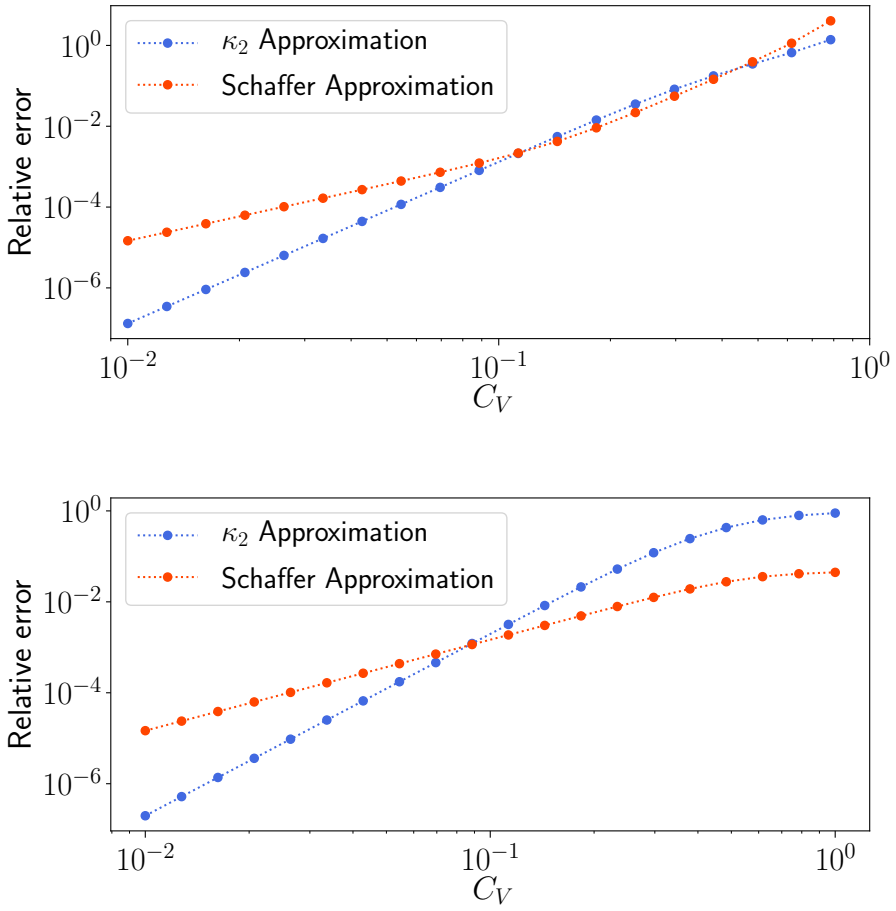

Figure 3.3: **Top:** Gamma neuron model. **Bottom:** PIF neuron modle. Relative error on the eigenvalue for the eigenvalue approximations derived by Schaffer et al. (2013) Eq.(3.23), and by Eq.(3.22) using the cumulant expansion as a function of C_V.

Chapter 4

Evaluation of spectral approximations

4.1 Transcient response of the population activity starting with a delta distribution $q(\tau, 0) = \delta(\tau)$

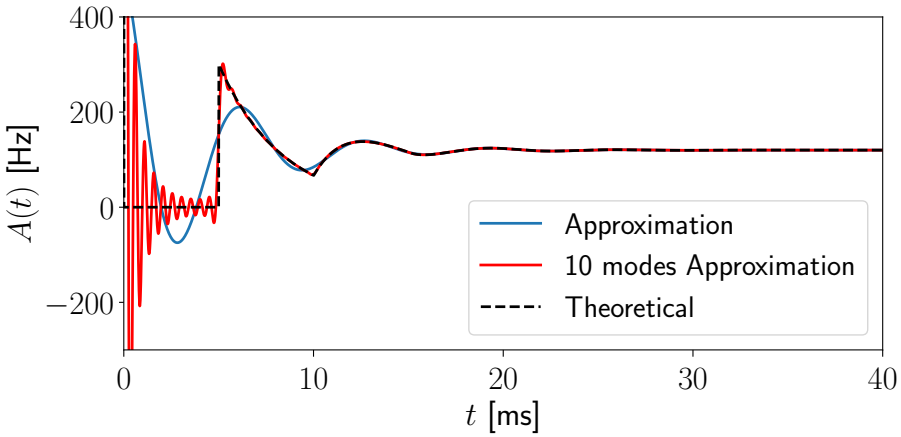

Figure 4.1: Activity $A(t)$ of a population of neuron of poisson neuron with absolute refractoriness Δ The approximation given by Eq.(2.25), and the 10 modes approximation is given by by Eq.(2.22) with $n = 10$. The parameters used are $h = h_0$, $\Delta = 5$ ms, and $\nu_{max} = 0.6\ kHz$ and the initial condition is $q(\tau, 0) = \delta(\tau)$

In this section we will look at the result of the approximation Eq.(2.38) for the gamma neuron model and for a population of Poisson neurons with absolute refractoriness. For the sake of simplicity we consider first a large homogeneous population of uncoupled neurons with a constant input potential.The initial distribution of the refractory density q is given by a delta peak $q(\tau, 0) = \delta(\tau)$, i.e all neurons spike at time $t = 0$.

As expected for the Poisson neuron with absolute refractoryness model, we need infinitely many modes to recover the exact initial distribution Fig.4.1. We will see later that keeping only the first mode is a good approximation for changes that are not too fast, which is not the case of a delta peak. Nevertheless Fig.4.1 one can see that we quantitatively reproduce the response i.e the oscillations of the activity with the approximation given by Eq.(2.38), and we even recover the shape of the first peak taking the 10 first mode of Eq.(2.22).
The Gamma neuron model has a finite number of modes Eq.(3.13) and we see on Fig.4.1 that we recover exactly the activity $A(t)$ taking the complete expansion.

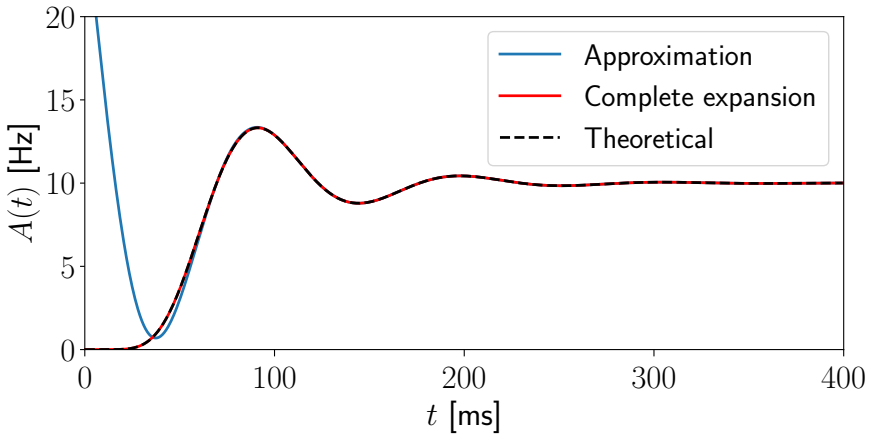

Figure 4.2: Activity $A(t)$ of a population of neurons having an ISI density given by the gamma distribution with $\beta = 100$ Hz and $\gamma = 10$ starting with a delta distribution $q(\tau, 0) = \delta(\tau)$. With the approximation given by Eq.(2.38), and the complete expansion given by Eq.(2.22)

4.2 Population response to time-dependent input

In this section we will study the response of a large population of uncoupled (i.e $J = 0$) Poisson neuron with absolute refractoriness to an external time dependent input potential $\mu(t)$. The differential equation for the input potential h is given by Eq.(1.1), and the firing rate of the Poisson neurons is given by $\Phi(h)$ Eq.(1.11). We will compare the population activity approximation given by Eq.(2.38), to the theoretical one computed as

$$A(t) = \Phi(h) \left(1 - \int_{t-\Delta}^{t} A(s)\mathrm{d}s\right) \tag{4.1}$$

We will use as an error measure the normalized root-mean-square deviation NRMS. The NRMS of predicted values $\hat{y}_t$ for times t of a variable y_t with variables observed over T times, is computed as the square root of the mean of the squares of the deviations normalized by the range of value of y

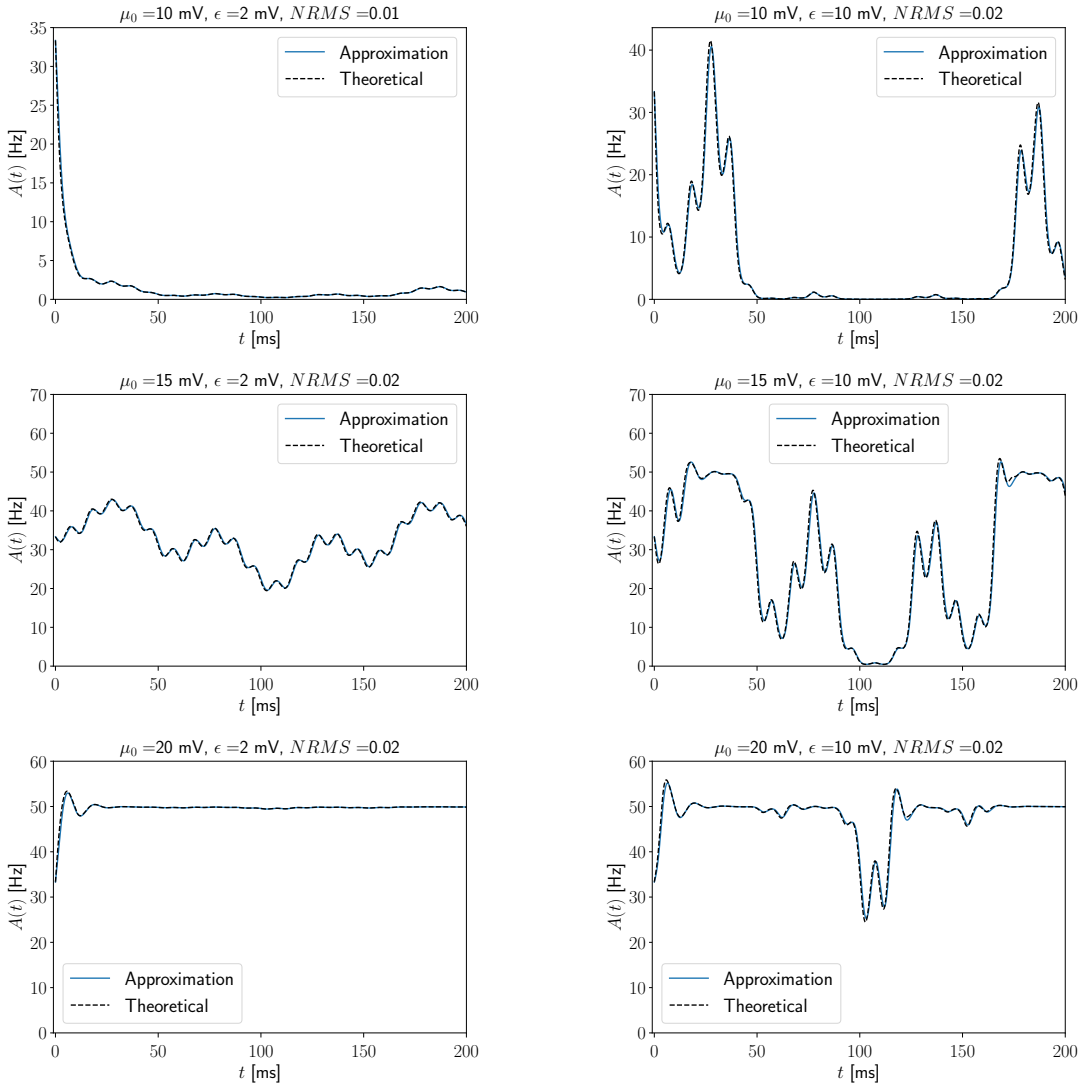

Figure 4.3: Response of a population of uncoupled Poisson neurons with absolute refractoriness to a fluctuating external input given by Eq.(4.4). For different amplitude ϵ of the oscillating function $f_{cos}(t)$(left: $\epsilon = 2$ mV, right: $\epsilon = 10$ mV)), for different baseline of the external potential input, top: $\mu_0 < h_0$, middle $\mu_0 = h_0$ and bottom: $\mu_0 > h_0$ The parameters of the neurons are $\nu_{max} = 100$ Hz, $\Delta = 10$ ms, $\beta = 1$ mV^{-1} , $h_0 = 15$ mV. The time constant of the input potential h is $\tau_m = 10$ ms.

$$NRMS = \frac{1}{y_{max} - y_{min}} \sqrt{\frac{\sum_{t=1}^{T} (\hat{y}_t - y_t)^2}{T}} \tag{4.2}$$

Our approximation Eq.(2.38) only keeps the slowest mode, so we expect that the theory breaks down for fast inputs. To study the accuracy of our approximation, we looked at

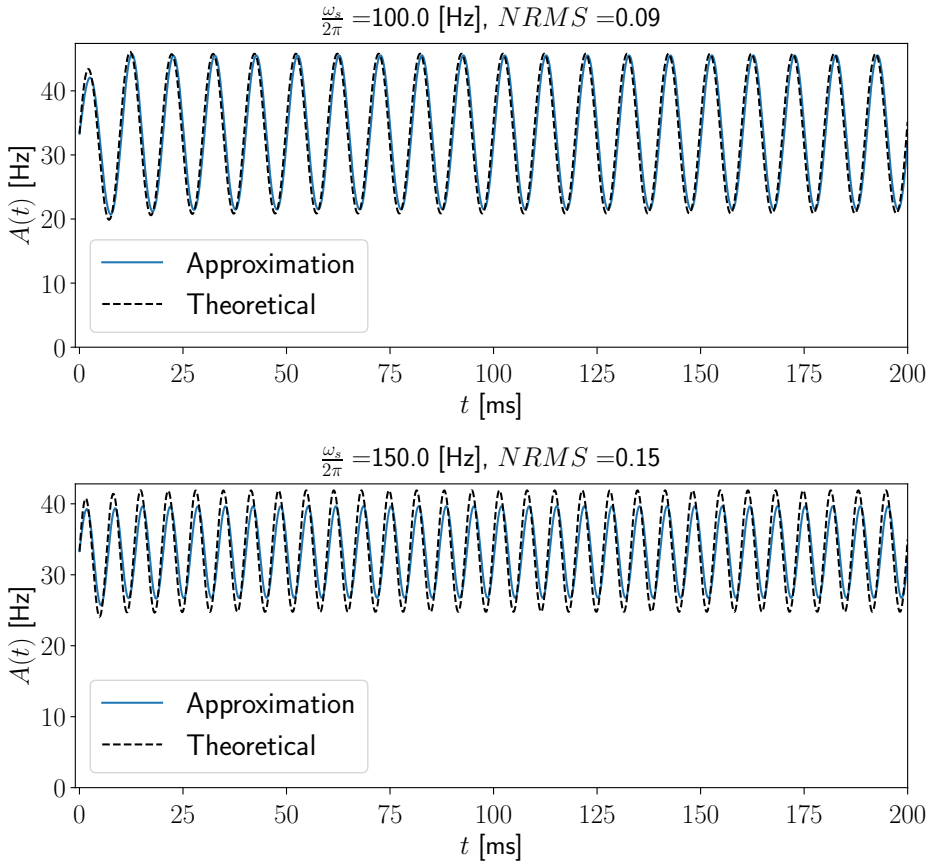

Figure 4.4: Population response to an oscillating input $\mu(t)$ with angular frequency ω_s (top: 100 Hz, bottom 150 Hz), for a large populations of uncoupled Poisson neurons with absolute refractoriness. The parameters of the neurons are $\nu_{max} = 100$ Hz, $\Delta = 10$ ms, $\beta = 1$ mV^{-1} , $h_0 = 15$ mV. The time constant of the input potential h is $\tau_m = 10$ ms.

the response of the model to a sinusoidal modulation of the external input potential $\mu(t)$ with an angular frequency ω_s

$$\mu(t) = \mu_0 + \epsilon \cos(\omega_s t) \tag{4.3}$$

The input potential was initialized as if the population activity was at a stationary state with $h(0) = \mu_0 = h_0$.
The results are summarized in Fig.4.5. For frequencies higher than 100 Hz, the NRMS becomes high thus the approximation does not hold anymore. On Fig.4.4, one can see that for a frequency of 150 Hz the activity amplitude of the approximation becomes lower than the theoretical one.
To study the population response to more complex signals we used as external input

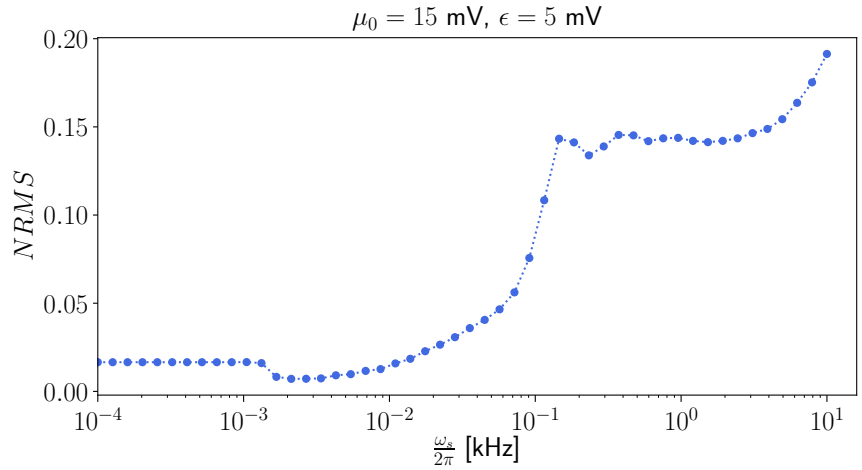

Figure 4.5: NRMS on the response of population of uncoupled Poisson neurons with absolute refractoriness as a function of the angular frequency ω_s of the sinusoidal modulation of the external input potential $\mu(t)$ Eq.(4.3). The parameters of the neurons are $\nu_{max} = 100$ Hz, $\Delta = 10$ ms, $\beta = 1$ mV^{-1} , $h_0 = 15$ mV. The time constant of the input potential h is $\tau_m = 10$ ms.

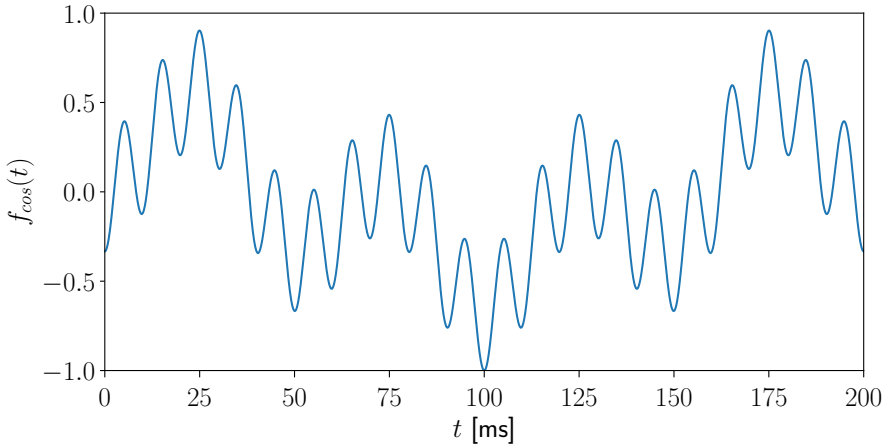

Figure 4.6: Mix of equal amplitude sinusoidal oscillation with different frequencies: 5, 20 and 100 Hz. $f_{cos}(t) = \frac{1}{3}\left(\cos(\omega_1 t) - \cos(\omega_2 t) - \cos(\omega_3 t)\right)$

$$\mu(t) = \mu_0 + \epsilon f_{cos}(t) \tag{4.4}$$

Where μ_0 and ϵ are constant and $f_{cos}(t)$ is a function composed of equal-amplitude sinusoidal oscillation with different frequencies. $f_{cos}(t)$ is represented of Fig.4.6. Fig.4.3 illustrates the response for different μ_0 and ϵ. In the sub threshold $\mu_0 << h_0$ the activity is shut down due the sigmoid rate function $\Phi(h)$. In the suprathreshold limit $\mu_0 >> h_0$ the activity goes toward the value $\frac{\nu_{max}}{1+\Delta\nu_{max}}$. Fig.4.7 illustrates the accuracy of the approximation for the different input. For the different input the NRMS stays below 2.5% which

highlight the validity of the approximation.

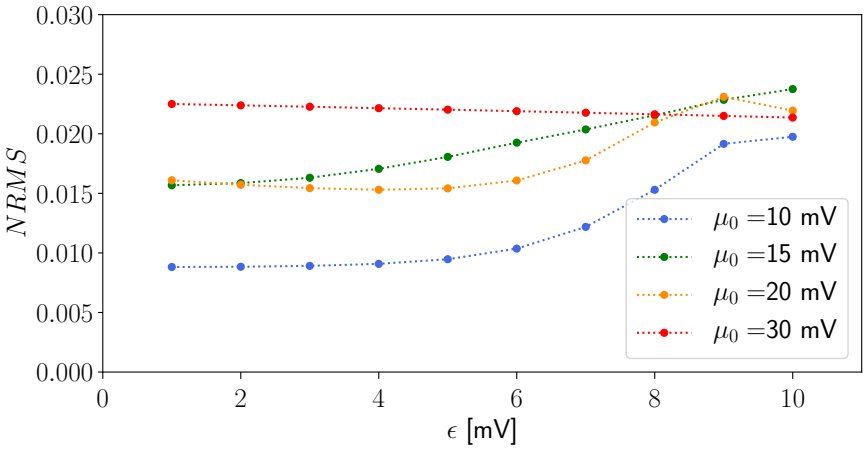

Figure 4.7: NRMS on the response of population of uncoupled Poisson neurons with absolute refractoriness to a fluctuating external input given by Eq.(4.4). For different amplitude ϵ of the oscillating function $f_{cos}(t)$, for different baseline potential μ_0. The parameters of the neurons are $\nu_{max} = 100$ Hz, $\Delta = 10$ ms, $\beta = 1$ mV^{-1} , $h_0 = 15$ mV. The time constant of the input potential h is $\tau_m = 10$ ms.

Finally we analyzed the response of the population to an abrupt change in the external input with a step function, from 15mV to $\mu(t) = \mu_0$ for $t > 0$. The response for two different value of μ_0 is shown on Fig.4.8. The response shows an oscillatory behavior, the amplitude of the oscillation increases with μ_0, as well as the NRMS as shown on Fig.4.9. As illustrated in Fig.4.8 even for large steps the response is rapidly well approximated by Eq.(2.38).

4.3 Effect of the refractoriness

To analyze the effect of the refractory period Δ on the transient response to an external input $\mu(t)$, we will compare the activity of a population of Poisson neuron with absolute refractoriness to an "equivalent" population of Poisson neuron. We know that the mean firing rate R of a population of Poisson neuron with absolute refractoriness Δ is given by

$$R = \frac{\Phi(h)}{1 + \Phi(h)} \tag{4.5}$$

Therefore the "equivalent" population of Poisson neurons is defined as a population of Poisson neuron with firing rate given by Eq.(4.5).
Fig.4.10 illustrates the difference in the response between a population of Poisson neurons with absolute refractoriness (blue line) and an "equivalent" population of Poisson neurons (red line) to abrupt change in the input potential $\mu(t)$. the external input $\mu(t)$ was a

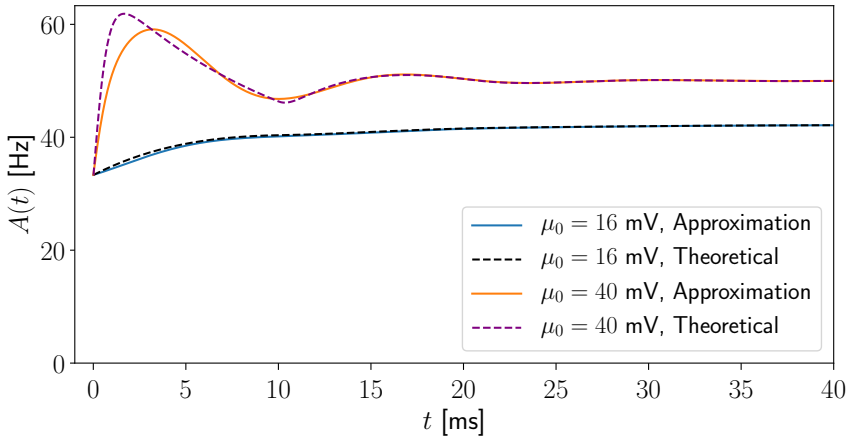

Figure 4.8: Transient response for a population of uncoupled Poisson neurons with absolute refractoriness, receiving as external input a step function $\mu(t)$. The parameters of the neurons are $\nu_{max} = 100$ Hz, $\Delta = 10$ ms, $\beta = 1$ mV^{-1} , $h_0 = 15$ mV.

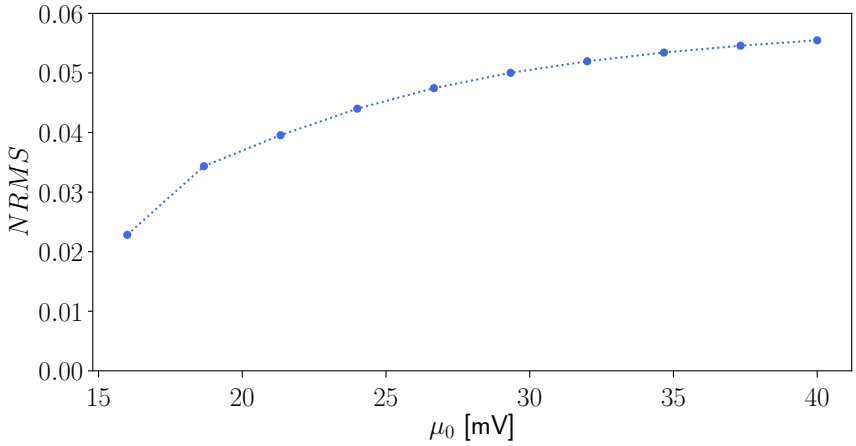

Figure 4.9: NRMS on the response of population of uncoupled Poisson neurons with absolute refractoriness to a abrupt change in the input potential $\mu(t)$. for different step from 15 mV to μ_0. The parameters of the neurons are $\nu_{max} = 100$ Hz, $\Delta = 10$ ms, $\beta = 1$ mV^{-1} , $h_0 = 15$ mV. The time constant of the input potential h is $\tau_m = 10$ ms.

step function changing every 50 ms (30 mV / 10 mV / 30 mV / 16 mV). Note that the blue line was obtained using the approximation Eq.(2.38), with an $NMRS = 0.02$. Contrary to the "equivalent" population of Poisson neuron, for the Poisson neurons with absolute refractoriness the response of the population activity to an abrupt change shows an oscillatory behavior in the approach to the new stationary state. The oscillations are absent in a quasi-stationary state and as expected the population activity become identical. When the input is lowered, the response of the population is delayed and doesn't show oscillations

and the response of the population of Poisson neurons with absolute refractoriness is a bit faster.

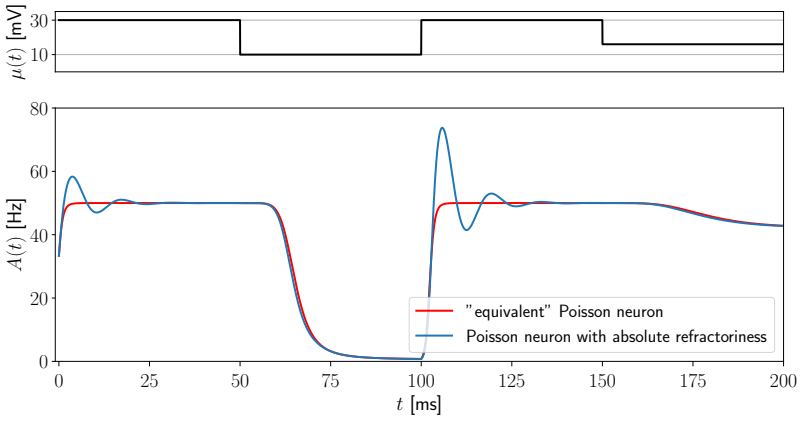

Figure 4.10: Transient response of the population activity (bottom) receiving as external input an step function $\mu(t)$ (top). The blue line correspond to the response of poisson neuron with absolute refractory period .The parameters of the neurons are $\nu_{max} = 100$ Hz, $\Delta = 10$ ms, $\beta = 1$ mV^{-1} , $h_0 = 15$ mV. The red line correspond to the "equivalent" population of Poisson neuron with firing rate given by Eq.(4.5)

Chapter 5

Population dynamics of coupled neurons

In this Chapter we consider an all-to-all coupled population of Poisson neuron with absolute refractoriness with firing rate given by $\Phi(h)$ Eq.(1.11). The dynamics of the input potential h are given by

$$\tau_m \dot{h} = -h + JA(t) + \mu(t) \tag{5.1}$$

where $\mu(t)$ is an external input potential and J is the coupling constant. For the sake of simplicity for the study, we will set some of the parameters constant. The parameters of the neurons are $\nu_{max} = 100$ Hz, $\Delta = 10$ ms, $\beta = 1$ mV^{-1} , $h_0 = 0$ mV, and the time constant of the input potential h is $\tau_m = 10$ ms.
We use as an error measure the normalized root-mean-square deviation Eq.(4.2)

5.1 Response to time dependent input

In this section we analyze the response similar to time dependent input, for a coupled population of excitatory neuron, i.e $J > 0$. As for the uncoupled case Section 4.2 we looked at the response of the model to a sinusoidal modulation of the external input potential $\mu(t)$ with an angular frequency ω_s Eq.(4.3)
The input potential was initialized as if the population activity was at a stationary state with $\mu_0 = -1$ mV and $J = 50$ mV$\cdot$ ms.
The results are summarize in Fig.5.2. Just as in the uncoupled case, for high frequency the approximation becomes poor. Fig.5.1 illustrates the response to a sinusoidal modulation with frequency 40 Hz.
We analyzed the response of the population activity to an abrupt change in the external input with a step function, from $\mu(0) = -2$ mV to a fixed value between -15 mV and 30 mV. Fig.5.3 illustrates the response for the extreme values of the step potential $\mu(t)$. For $\mu(t) = 30mV$ The response shows an oscillatory behavior, which is after 12 ms well approximated by Eq.(2.38). Because of the positive feedback the system goes to saturation,

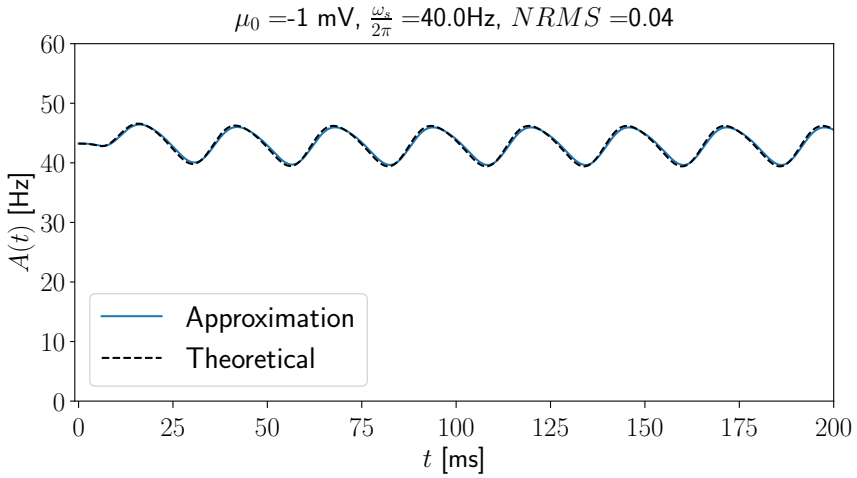

Figure 5.1: Population response to an oscillating input $\mu(t)$ with a frequency of 40Hz, for a large populations of coupled Poisson neurons with absolute refractoriness. The parameters of the neurons are $\nu_{max} = 100$ Hz, $\Delta = 10$ ms, $\beta = 1$ mV^{-1} and $J = 50$ mV$\cdot$ ms.

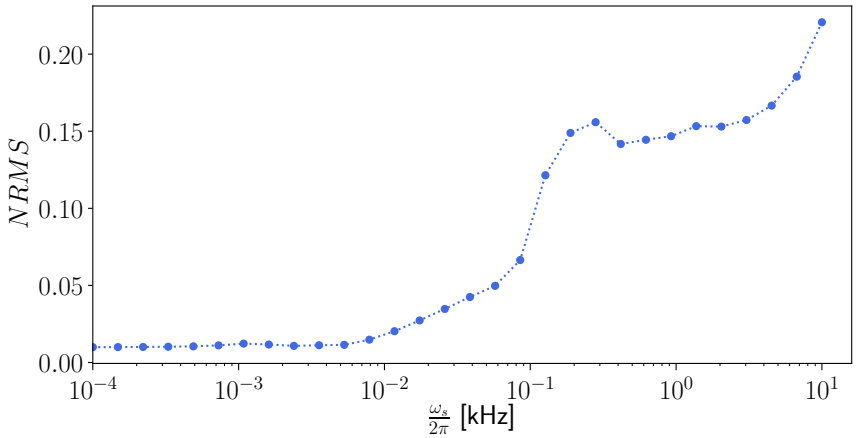

Figure 5.2: NRMS on the response of population of coupled Poisson neurons with absolute refractoriness as a function of the angular frequency ω_s of the sinusoidal modulation of the external input potential $\mu(t)$ Eq.(4.3). The parameters of the neurons are $\nu_{max} = 100$ Hz, $\Delta = 10$ ms, $\beta = 1$ mV^{-1} and $J = 50$ mV$\cdot$ ms.

the firing rate $\Phi(h)$ after the refractory period Δ goes immediately to $\nu_{max} = 100$Hz. With $\Delta = 10ms$ this yields to a rate of 50Hz as seen in stationary state. For the stationary state the rate is indeed given by $\frac{\Phi(h)}{1+\Delta\Phi(h)}$
For $\mu(t) = -15mV$ the coupling is not strong enough to compensate the strong negative external potential and the activity goes to 0. We see that the response of the approximation is a bit slower than the theoretical one. Fig.5.4 shows that the bigger the step in the external input potential the higher the NRMS.

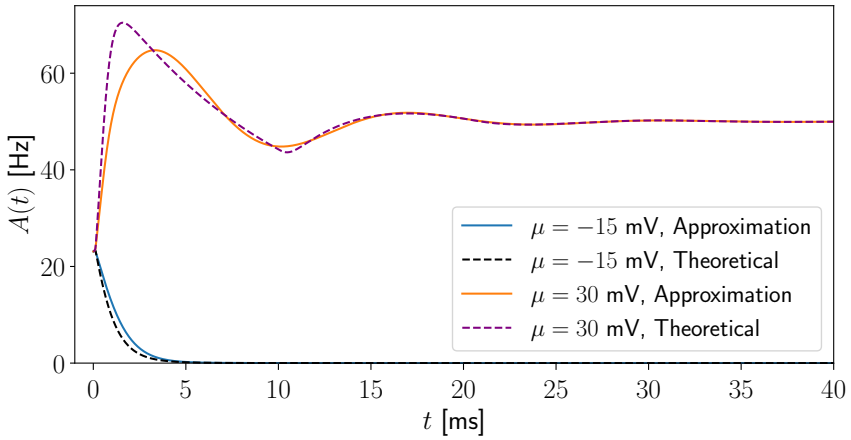

Figure 5.3: Transient response of the population activity for a population of coupled Poisson neurons with absolute refractoriness. receiving as external input a step function $\mu(t)$. The parameters of the neurons are $\nu_{max} = 100$ Hz, $\Delta = 10$ ms, $\beta = 1$ mV^{-1} , $J = 50$ mV$\cdot$ ms.

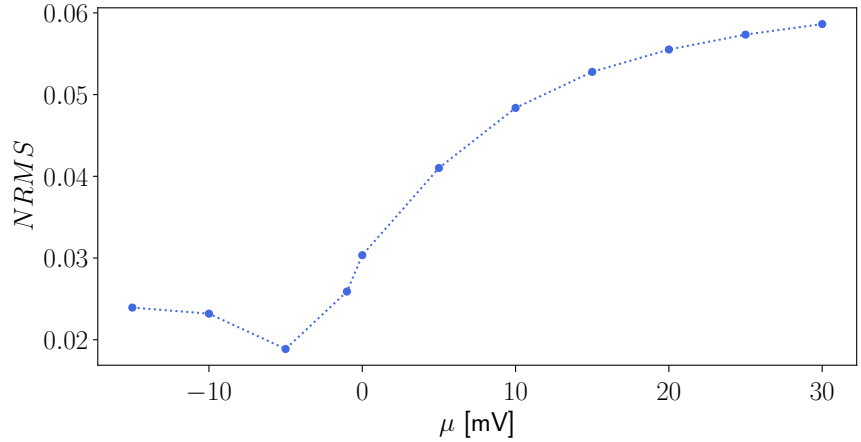

Figure 5.4: NRMS on the response of population of coupled Poisson neurons with absolute refractoriness to a abrupt change in the input potential $\mu(t)$. For different step from -2 mV to μ, -15 mV$\leq \mu \leq 30$ mV . The parameters of the neurons are $\nu_{max} = 100$ Hz, $\Delta = 10$ ms, $\beta = 1$ mV^{-1}, $J = 50$ mV$\cdot$ ms.

5.2 Fixed points of the dynamical system

In this section we are presenting preliminary results on the analysis of the fixed points of the model as a function of the coupling constant J and the external constant input μ.
We have a system of three differential equation $\dot{X}$, $\dot{Y}$ and $\dot{h}$ Eq.(2.28),(2.29),(5.1), we are looking for the fixed point of this system. When the activity reach an stationary value, this imply that $a_1(t) = 0$ an thus $X_{eq} = Y_{eq} = 0$ and

$$A_e q = \phi_0(0, h_{eq}) = \frac{\Phi(h_{eq})}{1 + \Delta\Phi(h_{eq}} \tag{5.2}$$

Note that looking at Eq.(2.28),(2.29), for $X = Y = 0$ and h_{eq} satisfying $\dot{h} = 0$ implies that $\dot{X} = \dot{Y}$=0. Therefore we can find the fixed point h_{eq} solving the equation

$$\tau_m \dot{h} = 0 = -h_{eq} + J\frac{\Phi(h_{eq})}{1 + \Delta\Phi(h_{eq}} + \mu \tag{5.3}$$

Fig.5.5 illustrates the solution of Eq.(5.3) for different J. We see that for $J = 250$ there are three fixed points (two stables and one unstable), but for $J = 50$ and $J = -50$ there is just one stable fixed point.
Eq.(5.3) might have more than one fixed point if there are local maxima or minima. To find the condition to have more than one fixed point, one can derive Eq.(5.3) with respect to h, this yields

$$x^2 + (2(1 + \Delta\nu_{max})) - J\beta)\, x + (1 + \Delta\nu_{max})^2 = 0 \tag{5.4}$$

Where $x = \exp(-\beta(h - h_0))$. A real solutions exist for x if $J > \frac{4(1+\Delta\nu_{max})}{\beta\nu_{max}}$, indeed, $J < 0$ yields to negative solutions for x which is impossible as x is strictly positive, and $0 < J < \frac{4(1+\Delta\nu_{max})}{\beta\nu_{max}}$ yields to complex solutions for x as the discriminant of Eq.(5.4) would be negative which is also impossible.

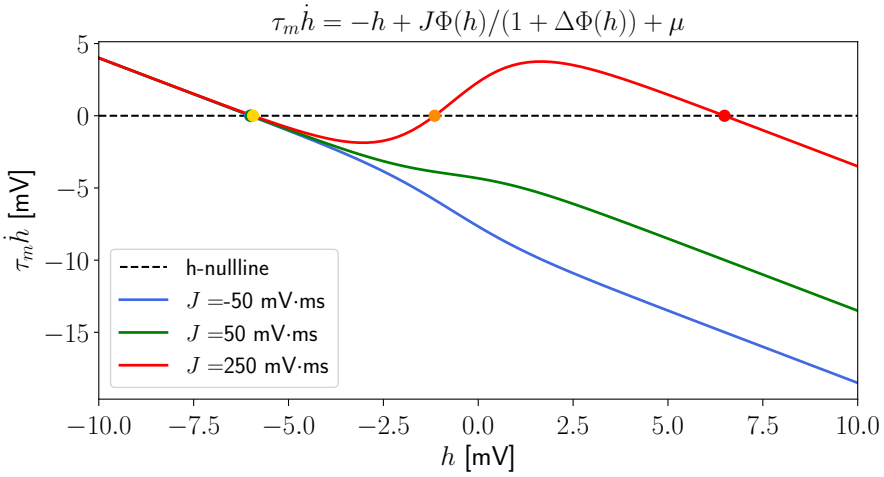

Figure 5.5: $\tau_m\dot{h}$ as a function of h for $mu = -6$ mV and for different J. The intersection with the $h - nullline$ corresponds to the fixed point of this dynamical system. For $J = -50$ and $J = 50$ there is only a "low firing rate" fixed stable point respectively indicates by a blue and a green dot, they are under the yellow dot corresponding to low firing rate for $J = 250$. For $J = 250$ there is also an "high friring rate" stable fixed point (red dot) and an "intermediate firing rate" unstable fixed point (orange dot).

One can see on Fig.5.5 that changing μ, just shift the line upward or downward. Thus for $J = 250$ there is a saddle node bifurcation when we decrease or when we increase μ. It is easy to compute numerically the values where the bifurcations occurs. Fig.5.6 summarize the derivation showing the number of fixed point as a function of J and μ, the three dots corresponds to the pair of parameters (J, μ) used in Fig.5.5.

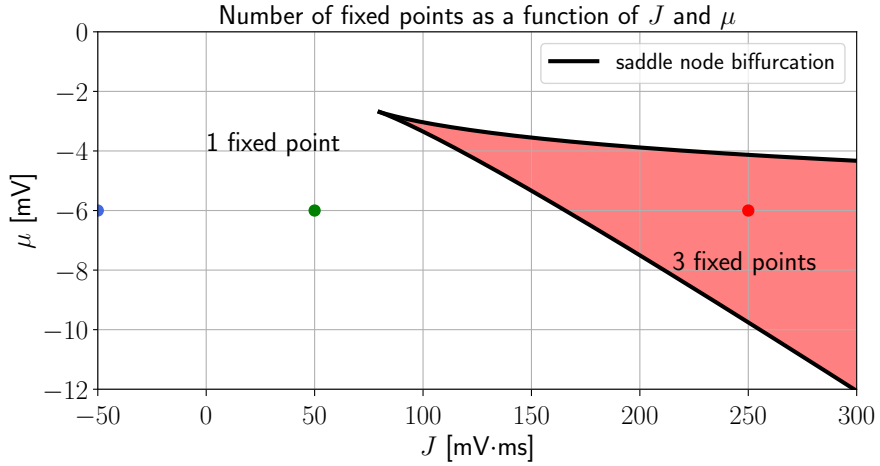

Figure 5.6: Number of fixed point and bifurcation for the parameters J and μ. The three dots corresponds to the pair of parameters (J, μ) used in Fig5.5.

To verify the stability of the different fixed points one can compute the Jacobian matrix of $(\dot{h}, \dot{X}, \dot{Y})$ evaluated in those fixed points.

$$J_f(h_{eq}, 0, 0) = \begin{pmatrix} \partial_h \dot{h} & \partial_X \dot{h} & \partial_Y \dot{h} \\ \partial_h \dot{X} & \partial_X \dot{X} & \partial_Y \dot{X} \\ \partial_h \dot{Y} & \partial_X \dot{Y} & \partial_Y \dot{Y} \end{pmatrix}_{|(h_{eq},0,0)} \tag{5.5}$$

This Jacobian matrix is directly obtained differentiating Eq.(2.28),(2.29),(5.1) with respect to h, X and Y and using the notation introduced in Eq.(2.30) to Eq.(2.37).

$$J_f = \begin{pmatrix} \frac{-1+J\partial_h\phi_0(0,h_{eq})}{\tau_m} & \frac{2J\Phi_r(h_{eq})}{\tau_m} & \frac{-2J\Phi_r(h_{eq})}{\tau_m} \\ \eta_r \frac{-1+J\partial_h\phi_0(0,h_{eq})}{\tau_m} & \alpha_r(h_{eq}) + \eta_r(h_{eq})\frac{2J\Phi_r(h_{eq})}{\tau_m} & -\alpha_i(h_{eq}) + \eta_r(h_{eq})\frac{-2J\Phi_r(h_{eq})}{\tau_m} \\ \eta_i \frac{-1+J\partial_h\phi_0(0,h_{eq})}{\tau_m} & \alpha_i(h_{eq}) + \eta_i(h_{eq})\frac{2J\Phi_r(h_{eq})}{\tau_m} & \alpha_r(h_{eq}) + \eta_i(h_{eq})\frac{-2J\Phi_r(h_{eq})}{\tau_m} \end{pmatrix} \tag{5.6}$$

If the real part of the three eigenvalues of the Jacobian matrix is negative then the fixed point is stable. The different eigenvalue are represented in the complex plane in Fig.5.7. We deduce that the "low firing rate" fixed point is a stable focus for $J = 50$,$J = -50$, $J = 250$, for $J = 250$ the "high firing rate" fixed point is also a stable focus and the "intermediate firing rate" fixed point is unstable.

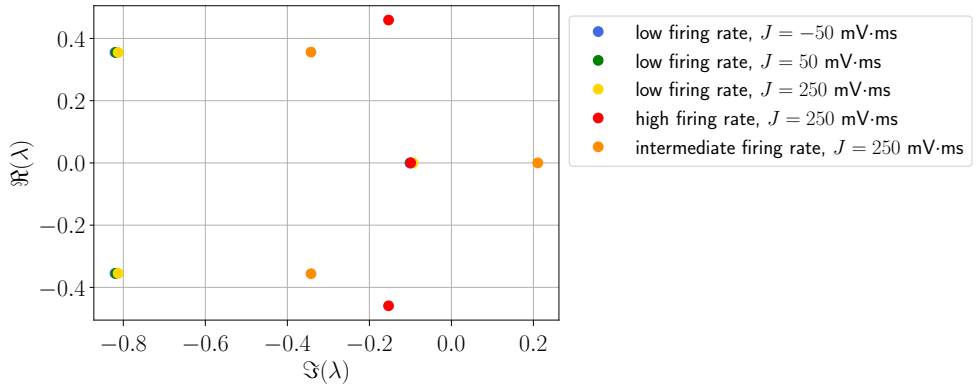

Figure 5.7: Representation in the complex plane of the three eigenvalues of the Jacobian Matrix Eq.(5.6) for different fixed points. The colors of the different fixed points correspond to the fixed points in Fig.5.5. Note that for $\Re\lambda \simeq -0.8$ the yellow, blue and green dots are superposed and for $\Re\lambda \simeq -0.1$ and $\Im\lambda \simeq -0.1$, the yellow, blue and green and red dots are superposed.

Chapter 6

Conclusions

We considered a large homogeneous populations of neurons modeled by a time dependent renewal process. We applied a probability density approach, which describes the evolution of the refractory density of states $q(\tau, t)$, where the age τ of a neuron is a state variable. We applied the eigenfunction expansion method presented in Section 1.4 to the operator of the refractory density, and derived from it a condition for the spectrum λ_n, Eq.(2.8). We also found a general expression for the biorthonormal basis of the refractory operator Eq.(2.6),Eq.(2.14) and Eq.(2.16). Keeping the slowest mode of the expansion of the refractory density, we derived a three dimensional system Eq.(2.28),(2.29) and(5.1), and a low dimensional firing rate equation Eq.(2.38). This three dimensional system has the advantages of being computationally efficient and mathematically tractable. For example in Section.5.2 we analyzed the fixed point of the derived system, in the case of Poisson neurons with absolute refractoriness.

To study the accuracy of our approximation we looked at the response of population of Poisson neuron with absolute refractory period Δ to time dependent input and compare it to the theoretical solution with the integral formulation. Chapter.4 emphasizes the validity of the approximation for low frequencies in both the uncoupled case and coupled case. The response to a step function is rapidly well approximated by Eq.(2.38).

They are nevertheless some limitations of the analytical results. For a general model defined by its hazard rate function, it's not always possible to find an analytical solution to the condition Eq.(2.8). That's why we tried to find an approximation of the first eigenvalue λ_1 as we want to keep only the two first mode. Using the cumulant expansion Section.(3.2) we found an approximation which seems to be valid for low C_V, and is close to the one obtained in [Schaffer et al. (2013)], but more general. Another limitation is that it is not always possible to derive an analytical form of the eigenfunctions, especially it is not easy to find a solution of the normalization condition Eq.(2.16), and also find an analytical form of the coupling coefficient. This has not been yet investigated, and would be a direction to continue this work. We also neglect in this model finite size effect, and the sparse coupling of neurons Schwalger et al. (2017).

Despite those limitations, the analytical results have many advantages. We obtained the expected response of large homogeneous population of Poisson neurons with absolute refractory period, to different external inputs potential. This simple model is very useful to study the effect of absolute refractoriness. Furthermore we derived a low dimensional firing rate dynamics of spiking neuron network from properties of individual neurons, which is not a phenomenological firing rate model. As a future work it would be interesting to use this model to analyze the interaction between different populations of excitatory and inhibitory neurons.

References

M. Augustin, J. Ladenbauer, F. Baumann, and K. Obermayer. Low-dimensional spike rate models derived from networks of adaptive integrate-and-fire neurons: Comparison and implementation. *PLOS Computational Biology*, 13(6):1–46, 06 2017. .

A. V. Chizhov and L. J. Graham. Population model of hippocampal pyramidal neurons, linking a refractory density approach to conductance-based neurons. *Phys. Rev. E*, 75 (1):011924, 2007.

A. V. Chizhov and L. J. Graham. Efficient evaluation of neuron populations receiving colored-noise current based on a refractory density method. *Phys. Rev. E*, 77(1):011910, 2008.

P. Dayan and L. F. Abbott. *Theoretical Neuroscience: Computational and Mathematical Modeling of Neural Systems*. The MIT Press, 1 edition, 2005.

W. Gerstner. Population dynamics of spiking neurons: Fast transients, asynchronous states, and locking. *Neural Comput.*, 12:43, 2000.

W. Gerstner and W. M. Kistler. *Spiking Neuron Models: Single Neurons, Populations, Plasticity*. Cambridge University Press, Cambridge, 2002.

W. Gerstner, W. M. Kistler, R. Naud, and L. Paninski. *Neuronal Dynamics: From Single Neurons to Networks and Models of Cognition*. Cambridge University Press, Cambridge, 2014.

E. R. Kandel, J. H. Schwartz, and T. M. Jessell. *Principles of Neural Science*. Mcgraw-Hill Professional, 4. a. edition, 2000.

B. W. Knight. Dynamics of encoding in a population of neurons. *J. Gen. Physiol.*, 59:734, 1972.

B. W. Knight, D. Manin, and L. Sirovich. Dynamical models of interacting neuron populations in visual cortex. *Robot Cybern*, 54:4–8, 1996.

S. Lefort, C. Tomm, J.-C. F. Sarria, and C. C. Petersen. The excitatory neuronal network of the c2 barrel column in mouse primary somatosensory cortex. *Neuron*, 61(2):301 – 316, 2009. .

M. Mattia. Low-dimensional firing rate dynamics of spiking neuron networks. *ArXiv e-prints*, 2016.

M. Mattia and P. Del Giudice. Population dynamics of interacting spiking neurons. *Phys. Rev. E*, 66:051917, 2002.

S. Ostojic and N. Brunel. From spiking neuron models to linear-nonlinear models. *PLOS Computational Biology*, 7(1):1–16, 01 2011. .

V. F. Prijs, J. Keijzer, H. Versnel, and R. Schoonhoven. Recovery characteristics of auditory nerve fibres in the normal and noise-damaged guinea pig cochlea. *Hearing Research*, 71 (1):190 – 201, 1993. .

H. Risken. *The Fokker-Planck Equation*. Springer, Berlin, 1984.

E. S. Schaffer, S. Ostojic, and L. F. Abbott. A complex-valued firing-rate model that approximates the dynamics of spiking networks. *PLoS Comput. Biol.*, 9(10):e1003301, 2013.

T. Schwalger. *The interspike-interval statistics of non-renewal neuron models*. PhD thesis, Humboldt-Universitat zu Berlin, Mathematisch-Naturwissenschaftliche Fakultat I, 2013.

T. Schwalger. An attempt to make an Eigenfunction expansion of the refrcatory density for renewal processes. *unpublished notes*, 2016.

T. Schwalger, M. Deger, and W. Gerstner. Towards a theory of cortical columns: From spiking neurons to interacting neural populations of finite size. *PLoS Comput. Biol.*, 13 (4):e1005507, 2017. .

C. van Vreeswijk. Stochastic models of spike trains. In S. Grun and S. Rotter, editors, *Analysis of Parallel Spike Trains*, chapter 1. Springer, 2010.

H. R. Wilson and J. D. Cowan. Excitatory and inhibitory interactions in localized populations of model neurons. *Biophys. J.*, 12(1):1, 1972.